Article

Logic-Based Modeling of Inflammatory Macrophage Crosstalk with Glomerular Endothelial Cells in Diabetic Kidney Disease

Krutika Patidar[1] and Ashlee N. Ford Versypt[1,2,3,*]

[1]Department of Chemical and Biological Engineering, University at Buffalo, The State University of New York, Buffalo, NY, USA
[2]Department of Biomedical Engineering, University at Buffalo, The State University of New York, Buffalo, NY, 14260, US
[3]Institute for Artificial Intelligence and Data Science, University at Buffalo, The State University of New York, Buffalo, NY, 14260, USA
[*]Correspondence: ashleefv@buffalo.edu

ABSTRACT Diabetic kidney disease is a complication in 1 out of 3 patients with diabetes. Aberrant glucose metabolism in diabetes leads to an immune response causing inflammation and to structural and functional damage in the glomerular cells of the kidney. Complex cellular signaling lies at the core of metabolic and functional derangement. Unfortunately, the mechanism underlying the role of inflammation in glomerular endothelial cell dysfunction during diabetic kidney disease is not fully understood. Computational models in systems biology allow the integration of experimental evidence and cellular signaling networks to understand mechanisms involved in disease progression. We built a logic-based ordinary differential equations model to study macrophage-dependent inflammation in glomerular endothelial cells during diabetic kidney disease progression. We studied the crosstalk between macrophages and glomerular endothelial cells in the kidney using a protein signaling network stimulated with glucose and lipopolysaccharide. The network and model were built using the open-source software package Netflux. This modeling approach overcomes the complexity of studying network models and the need for extensive mechanistic details. The model simulations were fitted and validated against available biochemical data from *in vitro* experiments. The model identified mechanisms responsible for dysregulated signaling in macrophages and glomerular endothelial cells during diabetic kidney disease. In addition, we investigated the influence of signaling interactions and species that on glomerular endothelial cell morphology through selective knockdown and downregulation. We found that partial knockdown of VEGF receptor 1, PLC-γ, adherens junction proteins, and calcium partially recovered the endothelial cell fenestration size. Our model findings contribute to understanding signaling and molecular perturbations that affect the glomerular endothelial cells in the early stage of diabetic kidney disease.

NEW & NOTEWORTHY We describe the findings of our novel analysis of signaling crosstalk between macrophages and glomerular endothelial cells in the early stage of diabetic kidney disease. Through a logic-based modeling approach, we identified key signaling molecules and interactions that regulate glucose-mediated inflammation in the glomerular endothelial cells and that damage endothelial fenestrations in the diabetic kidney. Our research revealed that the interaction among vascular endothelial growth factor A, nitric oxide, and junction proteins significantly affects the size of endothelial fenestrations.

KEYWORDS logic-based differential equations; protein signaling network; diabetic kidney disease; inflammation; glomerular endothelial cell

INTRODUCTION

Diabetic kidney disease (DKD) is a major microvascular complication in the kidney that affects about 30% of patients with type I diabetes and 40% of patients with type II diabetes (1). DKD causes reduced kidney function and may progress into chronic kidney disease (CKD) and end-stage renal disease (ESRD). Reports suggest that approximately 12–55% of cases of ESRD are due to diabetes (2). This imposes a high burden on the cost of living and quality of life. The high mortality in diabetic patients is often associated with CKD complications and progression to ESRD (3). Although diabetes management is one of the preventative treatments for DKD (4), the rising number of cases of type 1 and type 2 diabetes continues to increase the risk of DKD prevalence (1). There is still an urgent need to better understand the pathophysiology of DKD through effective and

preventative treatment strategies that can mitigate early signs of microvascular damage and DKD prevalence in diabetic patients (5).

Ongoing research suggests that DKD is caused by many complex and interlinked processes associated with high blood glucose and poor glycemic control. The hyperglycemic microenvironment has been linked to metabolic dysfunction in immune cells and inflammation. The microenvironment influences the activation of a pro-inflammatory stimulus such as exogeneous lipopolysaccharide (LPS), interferon-gamma (IFN-γ), or tumor necrosis factor-alpha (TNF-α) (6, 7), which in turn increases glucose uptake in immune cells (8). In the early stage of DKD development, immune cells like macrophages tend to polarize to a pro-inflammatory phenotype over an anti-inflammatory phenotype (8, 9). Together, the synergic action of pro-inflammatory mediators and increased glucose uptake contributes to dysregulated immune response and signaling (8). This dysregulated signaling enhances the expression of pro-inflammatory molecules, such as IL-6, TNF-α, IL-1β, and reactive oxygen species (ROS), which affect downstream macrophage response and activity (8, 9). These circulating pro-inflammatory molecules infiltrate the glomerular interstitium in the diabetic kidney (10) and cause microvascular damage to the glomerulus (6, 11). Recruitment of inflammatory macrophages and their mediators is a critical event in the pathophysiology of the early stage of DKD (10). We only have a superficial understanding of the highly complex and diverse molecular interactions in the diabetic kidney (6). Hence, a deeper analysis of glucose-mediated inflammatory mechanisms and pathways in the diabetic kidney can contribute to a comprehensive understanding of DKD development and progression.

Glomerular endothelial dysfunction is a pathological phenomenon that characterizes the early stages of DKD development and progression. In the functional unit of the kidney, glomerular endothelial cells (GECs) are early targets of diabetes-dependent inflammation and injury (2). Numerous studies suggest that activation of GECs in early DKD can dysregulate signaling pathways, promote intracellular hyperglycemia, elevate advanced glycation end products (AGEs) and their receptors, affect cell-cell adhesion, increase glomerular permeability, and promote the recruitment of inflammatory molecules (12). LPS-stimulated pro-inflammatory macrophages are involved in the activation of GECs *in vitro* (13). The inflammatory mediators and immune cells disrupt vascular endothelial growth factor (VEGF) expression, which plays a central role in maintaining vascular function of GECs and nitric oxide (NO) homeostasis (14, 15). Imbalanced VEGF expression causes uncoupling of endothelial nitric oxide synthase (eNOS), imbalance of NO, and loss of endothelial barrier integrity (14). The uncoupling of eNOS causes eNOS to produce NO as a product and ROS as a by-product, which leads to excessive oxidation of NO and reduces NO bioavailability in GECs (16). Hence, the uncoupling of eNOS is a crucial indicator of GEC activation and dysfunction. NO bioavailability within GECs has been associated with glomerular endothelial permeability (17, 18). An association between NO bioavailability and endothelial cell junction integrity has been suggested (19). In the kidneys, about 50% of the filtration through the glomerulus is dependent on GECs and the endothelial cell surface layer, which makes GECs an essential contributor to the glomerular permeability of the kidney (20). The permeability of GECs is dependent on the endothelial cell fenestrations or gaps, which are transcellular holes located through GECs and regulated by cellular junction proteins (21). Many biophysical models have shown that the spatial arrangement of the GEC fenestrations is relevant to the overall glomerular filtration rate of the kidney (22–24). Thus, changes in GEC fenestration width are considered markers of GEC dysfunction during DKD progression. Despite some experimental studies on GECs in healthy and diseased states, a direct mechanistic link between macrophage-dependent endothelial cell activation and dysfunction in the early stage of DKD is not fully understood (19).

In the present study, we built a protein signaling network (PSN) of interconnected pathways between two cell types—GECs and macrophages—to study glucose-mediated inflammatory mechanisms in DKD. A PSN depicts the relationship between interacting proteins using directional arrows (25). We used a computational approach to integrate published experimental evidence and protein signaling networks. However, modeling signaling networks with many interacting species can become complex and tedious. Ordinary differential equations (ODEs) are often used to model these biochemical networks (26–29), but these models rely on extensive data, parameter values, and knowledge of reaction kinetics. Alternatively, modelers have used logic-based modeling, fuzzy logic modeling, and extreme pathways analysis to study complex mammalian signaling networks (25, 30). These techniques require few or no parameters. For instance, a discrete logic model (Boolean model) successfully showed the changes in endothelial cell behavior and signaling due to extracellular micro-environments (31). A logic-based model (LBM) was used to gain a qualitative understanding of species expression, signaling pathways, and missing interactions involved in T cell activation (32). Furthermore, pathway analysis of differentially expressed genes and profiles in early DKD has helped understand critical pathophysiologic factors in DKD (33). However, each approach has limitations, including limited prediction of continuous dynamics (time course) in Boolean models, lack of realistic timescales in fuzzy logic analysis, and extensive data collection for pathway analysis. We were interested in predicting continuous signaling dynamics with limited data and mechanistic details. Previously, a hybrid modeling method has utilized the benefits of an ODE model to explain pathway interactions, while a qualitative logic-based model was used to define cell-cell interactions within a tissue environment (34). We applied a modeling technique that combines continuous dynamic ODE models with qualitative LBMs (30), which is termed a logic-based ordinary differential equations (LBODEs) model. Several research studies incorporated such transformation of logic-based models into systems of first-order ODEs (35, 36). Wittmann et al. have measured ligand concentrations and binding

affinities for the activation of T-cells by transforming a discrete Boolean model into ODEs using non-normalized Hill functions in Odefy toolbox (35). Logic-based formalism has also been used to reverse engineer complex biochemical networks from data and prior knowledge using metaheuristic optimization strategies, as seen in CellNOpt software (37, 38). NetFlux is another user-friendly software for developing dynamic logic-based computational models of biological networks (30). Kraeutler et al. presented the advantages of using LBODEs, especially when biochemical parameters are limited or unavailable; LBODEs were shown to identify unexpected network relationships, to generate experimentally testable predictions, and to agree with findings from a validated biochemical model (30). These softwares are readily available and easy to use. They enable the interpretation of biological networks and standardize the methods used to obtain biological insights, which may not be evident through discrete models (35). Therefore, we applied the LBODEs modeling approach to our PSN between macrophages and GECs stimulated under different conditions. To our knowledge, an analysis of signaling crosstalk between macrophages and GECs using an logic-based ordinary differential equations modeling technique has not been done previously. We predicted species dynamics, network relationships, and critical drivers of macrophage-dependent inflammation and glomerular endothelial dysfunction in the early stage of DKD.

The article has been organized as follows. We next explain the rationale behind the selected species and pathways in the network, model development and simulation steps, and experimental data selection for model fitting and validation. Then, we discuss the results from model fitting, validation, and predictions. The appendix provides the full list of equations used in this study.

METHODS

Network assembly

We formulated the PSN (Fig. 1) by manually assembling information from literature studies (6, 8, 14, 16, 31, 39–45) and pathway databases (46, 47). The PSN captures the signaling pathways and molecules that cause inflammation and dysfunction in two cell types: macrophages and GECs. The multi-cellular PSN has 30 species nodes and 40 interaction edges (Fig. 1). The green nodes are inputs or stimuli, the white nodes are regulatory nodes, and the blue nodes are model responses. The network has two stimuli: glucose (GLU) and LPS. LPS was selected because the *in vitro* data that we used for model fitting assumed LPS as an exogenous inflammatory stimulus as it is known to also induce a systemic immune response in humans (48); LPS was used as a representative systemic inflammatory stimulus like those triggered by diabetes. The network is stimulated with three different treatment conditions: GLU only, LPS only, and both GLU and LPS. Based on the logic-based formalism, two or more incoming arrows to a node are connected by an OR logic rule except where a red circle is placed denoting an AND logic rule (Fig. 1). An OR logic rule between two input nodes is used when either input can activate (black arrows) or inhibit (red flat-head arrow) the output node. The OR logic combines any number of input nodes acting on the same output; the corresponding reaction rules are listed independently but are composed into the OR operator in the LBODEs. An AND logic rule between two input nodes is used when both inputs are needed to activate the output node; a single reaction rule is defined for an AND logic rule. Fig. 2 shows representative examples of the possible types of interactions between nodes from Fig. 1.

Considering the complex nature of network interactions, we included signaling pathways involved in two main events in early DKD. These events include the release of pro-inflammatory molecules due to inflammatory macrophages and macrophage-dependent GEC activation and dysfunction. The rationale behind selecting these pathways and molecules is discussed further. In diabetes, immune cells like macrophages fail to metabolize glucose or regulate the efficient transport of glucose, which leads to intracellular hyperglycemia. Studies showed that this microenvironment initiates a pro-inflammatory signaling response downstream, governed by the activation of LPS and toll-like receptors (TLR) such as TLR4 (8, 9). In cell culture experiments, bacterial LPS is a representative pathogen-associated molecular pattern (PAMP) that allows mammalian cells to recognize bacterial invasion and trigger innate immune responses (8). In cultured macrophages, LPS was used to stimulate a robust inflammatory response, which initiates glucose-mediated inflammation in macrophages (8). Hence, LPS was considered one of the stimuli. LPS transduction signal is carried by activation of PI3K and AKT kinases, which mediate macrophage response, energy consumption, and energy metabolism (49). AKT is a primary substrate of PI3K and is associated with regulating inflammatory and energetic metabolic responses. Therefore, we speculate that PI3K and AKT are crucial in macrophage polarization in our network (8). Advanced glycation is one of the major pathways involved in the development and progression of different diabetic complications, including DKD (45). This protein glycation leads to advanced glycation end products (AGE), which activate and modify intracellular pathways through receptor-mediated signaling (45). The expression of AGE receptors (RAGE) is enhanced in cells like macrophages and endothelial cells during diabetes and inflammation. AGE and RAGE interaction on macrophages causes oxidative stress and activation of nuclear factor kappa B (NFκB) (45). The glycated proteins release ROS via activation of NADPH oxidase (40, 50). Moreover, aberrant PI3K-AKT signaling increases ROS levels through either direct modulation of mitochondrial bioenergetics or indirect production of ROS as a metabolic by-product

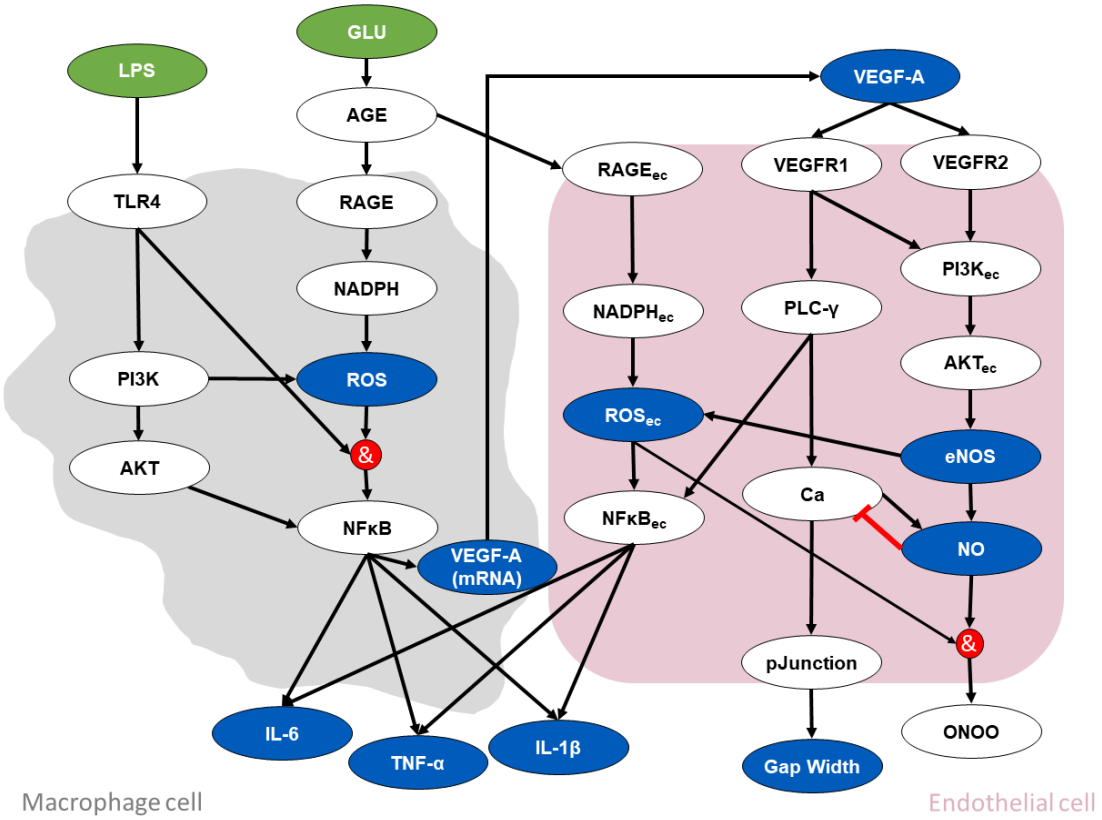

Figure 1: The multi-cellular protein signaling network of crosstalk between macrophages (left) and glomerular endothelial cells (right) stimulated with glucose (GLU) and lipopolysaccharide (LPS), a pro-inflammatory stimulus. Green nodes (ovals) are input nodes, blue nodes are output nodes, and white nodes are regulatory nodes. Black arrows are activating interactions, a red line with flat-head arrow is an inhibiting interaction, and red circles indicate logic *AND* gates. An *OR* logic rule connects two or more edges to a subsequent node throughout the network unless indicated otherwise by an *AND* logic gate. The subscript "ec" denotes an intracellular species expressed in endothelial cells. IL-6, TNF-α, IL-1β, and VEGF-A are protein levels expressed in extracellular space. ROS, ROSec, VEGF-A (mRNA), and NO are expressed within the cells. The Gap Width node denotes a fractional change in the glomerular endothelial cell fenestration size. The pJunction node represents the phosphorylated junction protein levels. TLR: toll-like receptor. AGE: advanced glycation end product. RAGE: receptor of advanced glycation end product. NADPH: nicotinamide adenine dinucleotide phosphate. NFκB: nuclear factor kappa B. IL: interleukin. TNF: tumor necrosis factor. PI3K: phosphoinositide 3-kinases. AKT: serine/threonine-specific protein kinases. ROS: reactive oxygen species. VEGF: vascular endothelial growth factor. VEGFR: vascular endothelial growth factor receptor. PLC: phospholipase C. NO: nitric oxide. ONOO: peroxynitrite. eNOS: endothelial nitric oxide synthase. Ca: calcium.

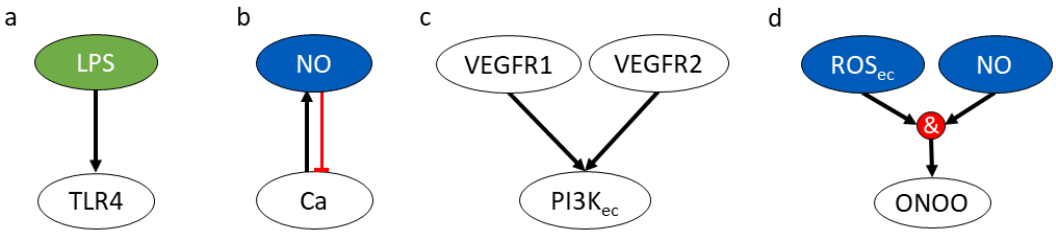

Figure 2: Logic-based formalism for a protein signaling network (PSN). The species interactions (a)–(d) are used as examples to explain logic-based model equations for the PSN in Fig. 1. Each of the following example description is followed by its corresponding reaction rule. (a) LPS activates TLR4: LPS ⇒ TLR4. (b) NO inhibits Ca: !NO ⇒ Ca, and Ca activates NO: Ca ⇒ NO. (c) VEGFR1 or VEGFR2 activate PI3K$_{ec}$ using an *OR* logic rule: VEGFR1 ⇒ PI3K$_{ec}$ *OR* VEGFR2 ⇒ PI3K$_{ec}$. (d) ROS$_{ec}$ and NO activate ONOO using an *AND* logic rule: ROS$_{ec}$ & NO ⇒ ONOO. A black arrow is an activating interaction, a red line with a flat-head arrow is an inhibiting interaction, and a red circle is a logic *AND* gate. LPS: lipopolysaccharide. TLR: toll-like receptor. PI3K: phosphoinositide 3-kinases. VEGF: vascular endothelial growth factor. VEGFR: vascular endothelial growth factor receptor. ROS: reactive oxygen species. NO: nitric oxide. ONOO: peroxynitrite. Ca: calcium. The subscript "ec" denotes an intracellular species expressed in endothelial cells.

(51). Hence, NADPH and PI3K-dependent ROS were considered in our network to gain a better perspective on mediators of ROS. Further, transcription factor NFκB contributes to the structural and functional changes observed in DKD, including pro-inflammatory macrophage polarization (45). NFκB is responsible for the expression of pro-inflammatory cytokines like IL-6, TNF-α, and IL-1β, inflammatory markers, growth factors, and adhesion molecules (6). The inflammatory cytokines and VEGF-A are responsible for the activation of glomerular endothelial cells in our network.

The macrophage-dependent VEGF-A expression is associated with the direct activation of GECs in our network. VEGF expression modulates the crosstalk between endothelial cells and macrophages (52). VEGF and its isoforms are critical to GECs. Excess VEGF contributes to DKD development and progression through disrupted signaling in GECs, whereas low VEGF levels can result in loss of capillaries and endothelial cells in the glomerulus (53). VEGF expression promotes endothelial cell development through NO modulation (53). Studies suggested that glucose indirectly regulates VEGF-A and signaling of its receptors (VEGFR1 and VEGFR2) in GECs (52, 54, 55). VEGFR1 receptor is a positive regulator of inflammation and immune cell recruitment via PLC-γ and PI3K pathways (42, 56, 57). The downstream signaling of VEGFR1 has yet to be fully understood, mainly due to its mild biological activity in culture (42). VEGF-A mediates signal transduction for cell proliferation, survival, migration, and enhanced vascular permeability via VEGFR2 receptor (15). VEGFR2-dependent signaling promotes eNOS activity, which produces NO, an important vasodilator in GECs (15). VEGF-A and VEGFR2 activity reduced in the GECs during diabetes (58). This phenomenon leads to perturbations in downstream signaling, eNOS uncoupling, and reduced NO bioavailability (59). As a result, excess ROS in GECs can react with available NO to form reactive nitrogen species like peroxynitrite (ONOO) (53, 60). In our network, the VEGF-dependent signaling pathway accounted for VEGF-A receptors VEGFR1 and VEGFR2, PLC-γ, eNOS, NO, ROS, and reactive nitrogen species expression. We also connected VEGF-dependent NO bioavailability with GEC dysfunction. We considered cell-cell junction proteins that hold adjacent GECs together, which modulate the passage of macromolecules, proteins, or infiltrating macrophages through the GEC layer. In activated GECs, the phosphorylation of these junction proteins, such as VE-cadherin, is regulated by calcium (Ca) expression via the PLC-γ pathway and NO expression (18, 61). The phosphorylation of VE-cadherin causes a loss of barrier integrity in GECs and triggers the opening of the intercellular junctions. VE-cadherin is shown as a pJunction node in our network. We posit that the junction opening or closing is directly related to the size of endothelial cell fenestration, shown as the Gap Width node in the network.

Data selection and extraction

The data for model fitting and validation was curated from selected published experimental studies based on the following criteria:

1. co-culture *in vitro* studies (13) were used to study cell-cell interaction between macrophages and GECs with some exceptions (8, 9, 62, 63),

2. bone-marrow derived macrophages (BMDM) from the diabetic subject and RAW 264.7 Murine macrophage cell line were most commonly considered (8, 9, 13, 63)

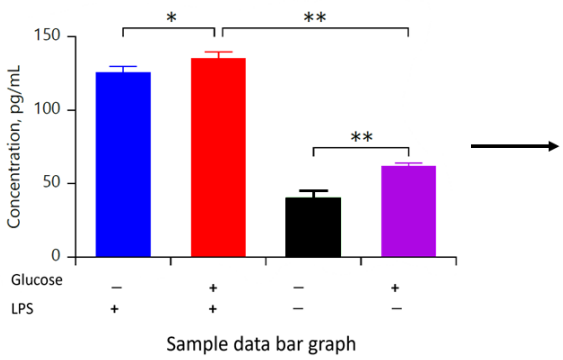

TR: GLU	TR: LPS	DA: TNFa	DV: TNFa	normalized
0	**0**	**0**	**45**	**0**
1	**0**	**0**	**45**	**0**
0	**1**	**0**	**45**	**0**
1	**1**	**0**	**45**	**0**
0	0	48	45	0
1	0	48	65	0.38
0	1	48	125	0.85
1	1	48	140	1

Sample MIDAS formatted csv file

Figure 3: Sample bar graph (left) of protein concentration at different glucose (GLU) or lipopolysaccharide (LPS) treatment conditions as found in published studies. The mean values and upper bounds were obtained using Webplotdigizer. These values were stored in a MIDAS-formatted comma-separated values (CSV) file, as shown in the table (right). TR:GLU and TR:LPS represents an active or inactive GLU and LPS treatment, respectively, where 0 represents inactive, and 1 represents active treatment. DA:TNFa and DV:TNFa represents the time (hours) and concentration (pg/ml) of TNF-α protein, respectively. Normalized values in the table were obtained using the method proposed in (25). Baseline values (black bar) were used for each treatment condition at the start of the experiment (time 0) in the table (bold text). The values at 48 hours correspond to the respective treatment conditions in the bar graph. For instance, the data obtained from the blue bar corresponds to the highlighted row in the table. TNF: tumor necrosis factor.

3. cells were stimulated with GLU concentration 5–30 mM and LPS concentration 0–0.1 µg/ml,

4. protein concentration from bar graph or data tables at the end of each experiment at several time points (6, 24, and 48 hours) for three treatment conditions GLU only, LPS only, and both GLU and LPS were collected where available (Fig. 3).

Co-culture experimental systems have gained popularity in the field, especially for studying and engineering complex multi-cellular synthetic systems and mimicking tissue structures to some extent (64). We used protein concentrations from individual cell culture studies on either macrophages or endothelial cells for IL-6, TNF-α, VEGF-A, ROS, eNOS, NO, and ROS_{ec} when data from co-culture systems were unavailable (8, 9, 62, 63). We extracted data from figures or tables in these publications (8, 9, 13, 62, 63, 65–70) using WebPlotDigitizer, a web-based data extraction software (71). We used ImageJ software (72) to quantify Western blot images from published papers when needed.

We normalized the curated data for two reasons: (1) to compare output from LBODEs model with data and (2) to pool data from multiple studies. It has been previously shown that it is essential to normalize the data and simulations in the same way to ensure uniformity between model output and data (73). Our model output lies between 0 and 1. Thus, we normalize the data in this range. Data normalization involves normalizing a data point with respect to the highest value in the series, but this can overemphasize data outliers and underweight minor and recurring differences in the series (25). Instead, we used a multi-step non-linear data normalization technique using an open-source software package, CellNOptR (38) proposed by Saez-Rodriguez et al. (25). To perform data normalization in CellNOptR, the data was stored as comma-separated values in a MIDAS-formatted file. Fig. 3 concisely represents sample bar graphs, data table and structure, and normalized values. The data normalization was performed as follows, (1) we normalized data between 0 and 1 by dividing each data value by the maximum value in the data series, (2) we calculated the relative change of each data point with respect to time 0, (3) transformed the relative change using a Hill function similar to (2), and (4) multiplied the transformed value and experimental noise (if any) to get the normalized data value. More detailed information on this normalization technique can be found in (25).

Logic-based ordinary differential equations model

We modeled the PSN using a LBODEs model. This modeling technique combines ODEs that are continuous functions of time with qualitative logic-based Boolean up- or down-regulation (i.e., activation or inhibition) using using normalized Hill functions (saturating terms) for the logic-based modeling portion as defined by Kraeutler et al. (30). The model equations were generated by the Netflux software package (74) upon providing the necessary interaction rules and species list. The Netflux package was used to compile the model equations and default parameters as MATLAB scripts, which were exported and used to run the model.

Each ODE defining the rate of change of normalized activity of a species A follows the same general form:

$$\frac{d\mathrm{A}}{dt} = \frac{\overbrace{y_{\max_{\mathrm{A}}} s(\mathrm{A})}^{\text{term 1}} \overbrace{-\mathrm{A}}^{\text{term 2}}}{\tau_{\mathrm{A}}} \tag{1}$$

where term 1 is the net activation rate (detailed further below), term 2 is the first-order de-activation rate, and τ_{A} is the characteristic time constant for the species. The initial condition is y_0. The net activation rate is scaled by $y_{\max_{\mathrm{A}}}$, the maximum normalized activation of species A.

The quantity $s(\mathrm{A})$ is the source of A from activating or inhibiting interactions that act alone or in combination through OR or AND logic operators. The activation or inhibition of output node species A is based on an interaction rule computed using a normalized-Hill function dependent on the signal from input node X. The activation function $f_{\mathrm{act}}(\mathrm{X})$ for how species X activates reaction j that produces A is

$$f_{\mathrm{act}}(\mathrm{X}) = W \frac{\beta \mathrm{X}^n}{K^n + \mathrm{X}^n}, \tag{2}$$

and the inhibition function $f_{\mathrm{inhib}}(\mathrm{X})$ for how species X inhibits reaction j that produces A is

$$f_{\mathrm{inhib}}(\mathrm{X}) = W - f_{\mathrm{act}}(\mathrm{X}) \tag{3}$$

where W is the weight of reaction j, n is the Hill coefficient for the reaction, EC_{50} is the half effect,

$$\beta = \frac{EC_{50}^n - 1}{2EC_{50}^n - 1}, \tag{4}$$

and

$$K = (\beta - 1)^{1/n}. \tag{5}$$

Multiple input signals to the same output node are automatically combined using an OR logical operator, unless indicated explicitly by an AND logical operator. Mathematically, $OR(a, b)$ is an OR logical operator for input a and b:

$$OR(a, b) = a + b - ab \tag{6}$$

$AND(a, b)$ is an AND logical operator for input a and b:

$$AND(a, b) = ab \tag{7}$$

We next illustrate the development a representative subset of the equations (eq. (8)-(11)) for the nodes and interactions illustrated in Fig. 2. The full network model interaction rules are provided in Table 1, and the corresponding equations are listed in the Appendix in eqs. (A1)–(A30).

A representative single activation interaction rule is LPS ⇒ TLR4 (Fig. 2a). The corresponding LBODE for tracking TLR4 is

$$\frac{d\mathrm{TLR4}}{dt} = \frac{y_{\max_{\mathrm{TLR4}}} f_{\mathrm{act}}(\mathrm{LPS}) - \mathrm{TLR4}}{\tau_{\mathrm{TLR4}}} \tag{8}$$

where the first term is the activation of TLR4 by LPS via a normalized Hill-type activation function, and the second term is the degradation of TLR4.

A representative single inhibition interaction rule is !NO ⇒ Ca (Fig. 2b), part of the negative feedback loop between NO and Ca. The corresponding LBODE for tracking Ca is

$$\frac{d\mathrm{Ca}}{dt} = \frac{y_{\max_{\mathrm{Ca}}} f_{\mathrm{inhib}}(\mathrm{NO}) - \mathrm{Ca}}{\tau_{\mathrm{Ca}}} \tag{9}$$

where the first term is the inhibition of Ca by NO via a normalized Hill-type inhibition function, and the second term is the degradation of Ca.

If a species is activated by two or more species, an AND or an OR logic operator is applied to combine the signals. A representative OR logic rule combining two activating signals is VEGFR1 ⇒ $\mathrm{PI3K_{ec}}$ OR VEGFR2 ⇒ $\mathrm{PI3K_{ec}}$ (Fig. 2c). The corresponding LBODE for tracking $\mathrm{PI3K_{ec}}$ is

$$\frac{d\mathrm{PI3K_{ec}}}{dt} = \frac{y_{\max_{\mathrm{PI3K_{ec}}}} OR\left(f_{\mathrm{act}}(\mathrm{VEGFR1}), f_{\mathrm{act}}(\mathrm{VEGFR2})\right) - \mathrm{PI3K_{ec}}}{\tau_{\mathrm{PI3K_{ec}}}} \tag{10}$$

A representative AND logic rule combining two activating signals is $\mathrm{ROS_{ec}}$ & NO ⇒ ONOO (Fig. 2d). The corresponding LBODE for tracking ONOO is

$$\frac{d\mathrm{ONOO}}{dt} = \frac{y_{\mathrm{max_{ONOO}}} AND\left(f_{\mathrm{act}}(\mathrm{NO}), f_{\mathrm{act}}(\mathrm{ROS_{ec}})\right) - \mathrm{ONOO}}{\tau_{\mathrm{ONOO}}} \tag{11}$$

Model parameters

The LBODEs model has parameters that can be divided into two categories: reaction parameters (W, EC_{50}, and n) and species parameters (τ, y_0, and $y_{\max}$). Reaction parameters including reaction weight W (constrained as $0 \leq W \leq 1$), half maximal effective concentration or half effect EC_{50} (constrained as $0.001 < EC_{50} < 0.84$), and Hill coefficient n (constrained as $1.4 \leq n \leq 4$) govern the interactions between species in the network. Each parameter's lower and upper bounds were based on prior knowledge and selected to satisfy eq. (4) and (5) (75). The parameter definitions, default values, and ranges were used as defined previously (30, 75). For a given interaction, the reaction weight W denotes the fraction of activation or inhibition of output species, and EC_{50} is the fraction of input required to induce a half-maximal effect on the output (30). The Hill coefficient n is a shape factor in the model (76). These reaction parameters define the normalized Hill activation or inhibition functions f in eq. (2)–(3). These functions are constrained as $f(0) = 0$, $f(1) = W$, and $f(0.5) = 0.5W$ in Netflux (30, 74). The species parameters include time constant τ (constrained $0.1 \leq \tau \leq 10$), initial value y_0, and maximal fractional activation of species $y_{\max}$ to describe the activity of a species in the network. The time constant (τ) parameter is arbitrary. This parameter modulates the signal propagation during early or late events and provides a rough estimate of the local dynamic behavior of the network (32). $y_{\max}$ is set to 1 by default and suggests the full activity of a species. $y_{\max}$ can be below or above a value of 1 to denote species knock-down or over-expression, respectively (30). The default values for these parameters, as generated by Netflux, are $W = 1$, $EC_{50} = 0.5$, $n = 1.4$, $\tau = 1$, $y_0 = 0$, and $y_{\max} = 1$. The model input (GLU or LPS or both) is 0 when inactive and 1 when fully active.

Model simulation

The model was simulated with default parameters for treatment conditions: $W_{\mathrm{GLU}} = 1$ and $W_{\mathrm{LPS}} = 0$ for GLU only, $W_{\mathrm{GLU}} = 0$ and $W_{\mathrm{LPS}} = 1$ for LPS only, and $W_{\mathrm{GLU}} = W_{\mathrm{LPS}} = 1$ for both GLU and LPS. However, the model predictions based on default parameters were only qualitative and not fitted to the data. The model parameters are not available in the literature, and not all parameters have biochemical relevance in this model. Hence, we optimized the model parameters against the calibration datasets for each treatment condition. Prior to model optimization, we performed a structure identifiability and observability analysis, and a variance-based sensitivity analysis. We performed an identifiability analysis to eliminate any uncertainty due to non-identifiable parameters in our model. Assessing the model's structural identifiability and observability helps detect any structural issues before model calibration (77, 78). We also performed a variance-based sensitivity analysis using Sobol's method to identify the most influential parameters that affect the model response significantly.

The structure identifiability and observability for LBODE model was performed in STRIKE-GOLDD before model calibration (79). The structure identifiability analysis evaluates the possibility of determining the parameter values from output measurements, whereas the observability analysis describes the ability to infer the dynamic variables of the model from the model output (77). The structural identifiability is completely defined by the model equations and input-output mapping and disregards the limitation of data quantity or quality (77, 78, 80). A Full Input-State-Parameter Observability (FISPO) algorithm in STRIKE-GOLDD was used to perform a joint structure identifiability of all model parameters (W, n, EC50, tau), and observability of all dynamic variables. The observability of the model variables (states, parameters, and inputs) is determined by calculating the rank of a generalized observability-identifiability matrix using Lie derivatives (81). The FISPO analysis yields a full rank for each computed Lie derivative and suggests that the LBODE model is observable and unknown parameters (W, n, EC50, tau) are structurally identifiable when initial states are known. Further details on the use of the STRIKE-GOLDD software package and the FISPO algorithm can be found in (77, 79, 81).

We used Sobol's method to perform a global sensitivity analysis of the model parameters. We used the UQLab toolbox (82) to perform the Sobol sensitivity analysis (83) in Matlab. We assessed the effect of reaction weight (W), Hill coefficient (n), half effect (EC_{50}), and time constant (τ) on the model response. First, we sampled each parameter from a specified range as suggested in an uncertainty quantification study previously (75). W, n EC_{50}, and τ were constrained between (0.8,1), (1.4, 4), (0.4, 0.6), and (0.5, 10), respectively. A Monte Carlo estimator in the UQLab sensitivity analysis toolbox was used to sample from the parameters in respective ranges. The sensitivity indices were computed using Sobol pseudo-random sampling (e.g. SOpts.Sobol.Sampling = 'Sobol') (82, 83). The sample size for Monte Carlo estimation (SobolOpts.Sobol.SampleSize) was set to 1000. The sample size was chosen based on the optimum computation time to run a global sensitivity analysis on 150 parameters. The Sobol sensitivity analysis computes sensitivity indices for scalar output quantities (84). Therefore, we chose

the predicted response of ROS, IL-6, TNF-α, IL-1β, VEGFA, ROS_{ec}, NO and eNOS at 48 hours as our scalar quantity of interest. We computed the first-order (Appendix Fig. A1-A4) and total Sobol sensitivity indices (Appendix Fig. A5-A8) for the quantity of interest, plotted these sensitivity indices for each parameter, and selected the most sensitive parameters that had a total Sobol sensitivity index above a given threshold or cut-off value. It is challenging to identify a single cut-off value for all the parameters (W, n EC_{50}, and τ). Therefore, we assumed a different threshold value for each parameter set. The total order Sobol sensitivity index within 10% of the maximum sensitivity index was fixed as the threshold for each parameter set. A total of 82 parameters were identified as sensitive and were optimized against the calibration dataset. The non-sensitive parameters were set to their default parameter values as mentioned previously. More information on the use of UQLab toolbox for sensitivity analysis can be found in the user manual (83).

The total order sensitivity indices corresponding to reaction parameters (W, n, and EC_{50}) and time constant (τ) are provided in the Appendix Fig. A5-A8. The sensitive parameters were optimized using a multi-start non-linear least squares parameter optimization method. We sampled 100 parameter start values using the Latin hypercube sampling technique (85). Each subset of parameter start values was optimized using the *fmincon* estimator in MATLAB. *fmincon* minimizes the objective function, which is the sum of squared error (SSE) between model prediction and published data (Fig. 3). The SSE is computed between model response and observed response for IL-6, TNF-α, IL-1β, VEGF-A, ROS, ROS_{ec}, NO, and eNOS at available time points. First, we performed a multi-start optimization of sensitive W, n, EC_{50}, and τ parameters for GLU only condition, where $W_{GLU} = 1$ and $W_{LPS} = 0$. For GLU only condition, initial values (y_0) of VEGF-A, NO, and eNOS were set to 1 to depict relative downregulation. It is relevant to note that the parameter optimization was carried out sequentially in the order of occurrence of species nodes in the network to avoid bias from multiple data points. For GLU only condition, model parameters governing the expression of ROS, ROS_{ec}, NO, eNOS, and VEGF-A were fitted against data before fitting the parameters for IL-6, TNF-α, and IL-1β response. The optimized reaction parameters (W, n, and EC_{50}) were fixed across different treatment conditions (GLU only, LPS only, both GLU and LPS). The sensitive τ parameters were re-calibrated for each treatment condition as the strength of the input signal affects rapid or delayed species response. These optimized model parameters are provided in Table 1 and 2.

We also identified uncertainty in estimated parameters. The parameter uncertainty is often defined by estimated confidence intervals for the best-fit parameters. The parameter optimization step provides 100 best-fit parameter sets for each optimization run and an optimal parameter set that gives the least SSE between prediction and data. To quantify parameter uncertainty, we computed the posterior distributions by running a large number of simulations on the best-fit parameter sets. We only sampled the best-fit parameter sets that were within an acceptable limit (20%) of the lowest SSE. A Monte Carlo (MC) sampling technique was used to sample 5000 parameter sets for each treatment condition. The summary statistics such as mean and standard deviation from these simulated posterior distributions were used to compute the 95% confidence interval. We simulated the model using optimal parameters and visually compared it with the mean prediction obtained from the posterior distributions. The statistical analysis of posterior distributions through estimated confidence intervals and visual checks allowed us to understand the extent of uncertainty in the estimated parameters.

Furthermore, the model simulations captured the normalized response of IL-6, TNF-α, IL-1β, ROS, ROS_{ec}, VEGF-A, eNOS, NO, pJunction, and change in Gap Width. In our study, we curated the biochemical data from multiple published sources. The normalized data were used to train the predicted response. Furthermore, the predictions generated by the fitted model for short-term exposure to GLU and LPS were also validated by independent *in vitro* data sets that were not used in model fitting.

Model assumptions

- Literature suggests a higher polarization of the pro-inflammatory phenotype of macrophage cells during early stages of DKD (8). We considered a pro-inflammatory phenotype of macrophages expressing pro-inflammatory species and ignored anti-inflammatory species for simplicity.
- GECs comprise a negatively charged matrix, the glycocalyx, which also contributes to endothelial permeability (2). We only focused on the glomerular endothelial cell layer as we studied GEC signaling and dysfunction. However, glycocalyx signaling and characteristics are not part of this study.
- AGEs are mediators and drivers of diabetic complications (13, 86). We assumed that glucose directly regulates AGE activation in our network. The mechanism regulating glucose-dependent AGE activation is not part of this study.
- The interaction kinetics across different endothelial cell lines are assumed to be the same, but protein levels of species may differ across cell lines (15). This has been previously considered in other models where data from different endothelial cell lines were curated due to the lack of studies on a specific cell line.
- The protein signaling network considers only two types of cells: macrophages and GECs. These cells are stimulated by GLU and LPS, which mimic hyperglycemic and inflammatory responses during the early stages of DKD, respectively.

Using a fixed physiological range allowed us to extract protein expression data from studies performed under similar treatment conditions. We assumed that full activation of GLU stimulus (i.e., $W_{GLU} = 1$) is analogous to a hyperglycemic range between 25-30 mM and full activation of LPS ($W_{LPS} = 1$) is the same as an active LPS treatment in cultured cells (0.1 μg/ml).

Model environment and specifications

The model was developed with the help of multiple software packages supported in MATLAB and R. The model was simulated, fitted, and validated in MATLAB. The ODEs were generated with the Netflux package and solved using the ode23s function in MATLAB. The data were normalized using the *normaliseCNOlist* function in CellNOptR in R (87). The model structural identifiability and obersvability analysis were performed using STRIKE-GOLDD software package in Matlab (79). The sensitivity analysis package from the UQLab toolbox (82, 83) was used to perform global sensitivity analysis in Matlab. The parameter optimization and uncertainty quantification were performed using the optimization toolbox in MATLAB (88). The *fmincon* estimator was used from the optimization toolbox to optimize model parameters and compute the Hessian matrix.

RESULTS AND DISCUSSION

Model fitting and validation

The normalized-Hill differential equations logic-based modeling approach was applied to the macrophage and glomerular endothelial cell signaling network. The model was fitted against normalized biochemical data for three different treatment conditions; only GLU stimulus is active (Fig. 4), only LPS stimulus is active (Fig. 5), or both GLU and LPS stimuli are active (Fig. 6). The model was simulated for short-term exposure (48 hours) to GLU or LPS based on the co-culture analysis in most published studies, with a few exceptions. The intercellular response variables like IL-1β and VEGF-A were fitted to co-culture data from macrophages and GECs (13). The intracellular response variables like IL-6, TNF-α, and ROS in the macrophage network were fitted to macrophage cell culture data (9, 63), whereas variables like ROS_{ec}, eNOS, and NO in GECs were fitted to endothelial cell culture data (62, 65, 67). We observed a visual and quantitative agreement between mean predictions (dashed line) from 5000 Monte Carlo simulations and optimal fit (blue solid line) except for slight deviations observed in IL-1β (Fig. 4c, 6c) and NO response (Fig. 6g). We observed narrow confidence intervals (95%) for each fitted response for the three treatment conditions.

The model was simulated with GLU treatment, where the glucose stimulus was active and the LPS stimulus was inactive. We observed that GLU treatment significantly upregulated pro-inflammatory cytokine IL-6, TNF-α, and IL-1β as early as 6 hours of treatment (Fig. 4a- 4c). This upregulation of pro-inflammatory cytokines can further augment the phenotypic switch towards the pro-inflammatory state in macrophages in the early stage of DKD. GLU treatment significantly downregulated VEGF-A secretion by macrophages (Fig. 4d). On the contrary, studies performed in diabetic subjects showed a systemic upregulation of VEGF levels. Our observations suggest that another stimulus and regulatory species may be involved besides GLU. In the LBODE model, macrophages are the only source of VEGF-A secretion, which could explain this contradictory observation. The downregulation of VEGF-A activity caused the downregulation of eNOS and reduction in NO bioavailability in GECs (Fig. 4f, 4g). Although our network model considers a simplified VEGF-dependent eNOS/NO pathway, it efficiently captures the glucose-mediated NO downregulation. To monitor the downregulation of a species, the initial value of y_0 was set at 1. Based on model predictions and literature evidence, GLU stimulation alone significantly upregulates ROS activity in both macrophages and GECs, Fig. 4e, 4h. In GECs, uncoupling of eNOS from its pathway triggered an over-expression of ROS_{ec} as a by-product. This upregulation of ROS_{ec} is associated with a simultaneous downregulation of NO and upregulation of ONOO in our model. In macrophages, ROS was upregulated due to glucose-mediated upregulation of AGEs and NADPH.

The model was stimulated with LPS treatment, where the LPS stimulus was active and the GLU stimulus was inactive (Fig. 5). LPS stimulus is a pro-inflammatory stimulus that upregulates inflammatory cytokines like IL-6, TNF-α, and IL-1β in our network. The activity of IL-6, TNF-α, and IL-1β increased 6 hours after activation by LPS stimulus in our network (Fig. 5a-5c). IL-6, TNF-α, and IL-1β achieve 50% of maximum activation much faster as compared to GLU only treatment. The fitted model predicts a slight increase in TNF-α expression at 6 hours. Multiple reactions and reaction parameters are responsible for TNF-α activity. NFκB transcription factor in macrophages and $NF\kappa B_{ec}$ transcription factor in GECs are responsible for activation of TNF-α. The fitted half-effect (EC_{50}) parameters for these two reactions were 0.4 and 0.84, which affects shift in TNF-α activity. LPS is a pro-inflammatory stimulus and a more potent regulator of pro-inflammatory cytokines. We observed that LPS stimulus alone upregulated VEGF-A activity in macrophages via PI3K-AKT and NFκB pathway in our network. The upregulated VEGF-A activates VEGF receptors on GECs (Fig. 5d). As mentioned, the VEGF-A protein can initiate downstream signaling through competitive binding to its receptors (VEGFR1, VEGFR2). Further, VEGF-A upregulation caused increased eNOS and NO activity (Fig. 5f, 5g). ROS expression was upregulated due to the PI3K-dependent pathway in macrophages

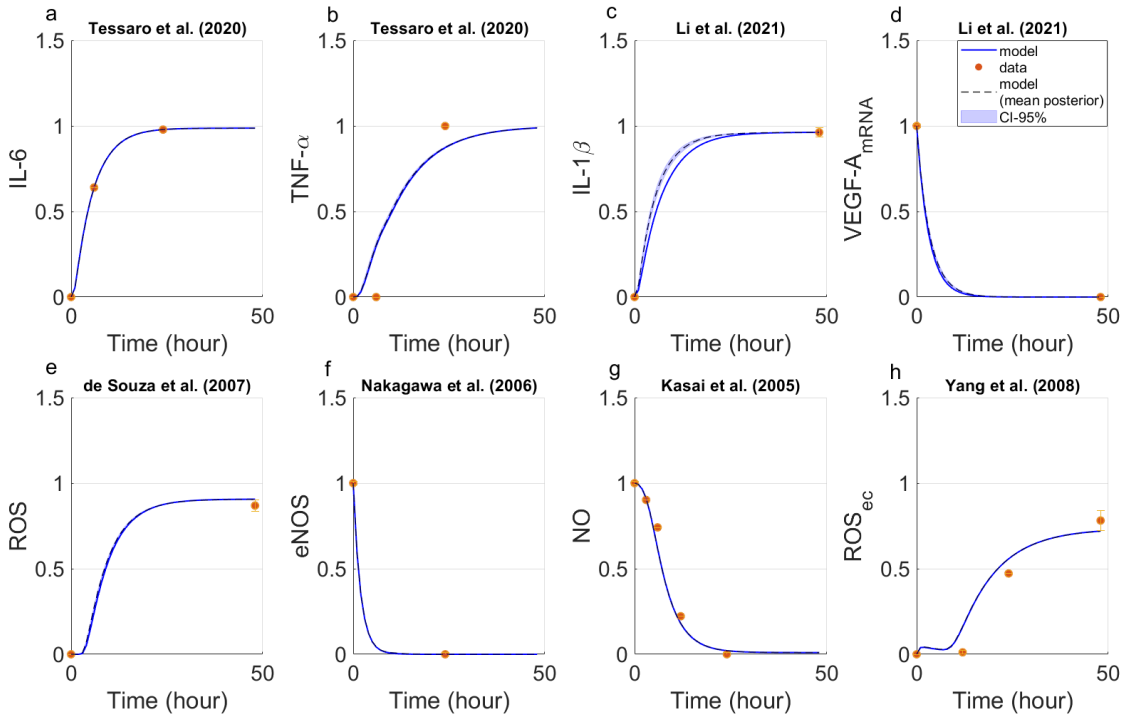

Figure 4: Network model fitted to biochemical data from (9, 13, 62, 63, 65, 67) upon stimulation with glucose (GLU) for 48 hours ($W_{\mathrm{GLU}} = 1$ and $W_{\mathrm{LPS}} = 0$). A semi-quantitative comparison of optimal model response against normalized protein levels of (a) IL-6, (b) TNF-α, (c) IL-1β, (d) VEGF-A (mRNA) levels, (e) ROS fluorescence, (f) eNOS, (g) NO, and (h) $\mathrm{ROS_{ec}}$. The optimal model prediction is shown as a blue solid line, mean prediction is shown as a dashed line, data are shown as orange points, and the 95% confidence region is shown as a blue-shaded region. Species activity above half-maximal activity (0.5) denotes relative upregulation, and species activity below half-maximal activity (0.5) denotes relative downregulation. The subscript "ec" denotes intracellular expression in glomerular endothelial cells. IL: interleukin. TNF: tumor necrosis factor. ROS: reactive oxygen species. VEGF: vascular endothelial growth factor. NO: nitric oxide. eNOS: endothelial nitric oxide synthase.

(Fig. 5e) and eNOS-dependent pathway in GECs (Fig. 5h). Although we have limited observed data at multiple time points for VEGF-A, ROS, eNOS, and NO activity, we can still gain insight into the downstream effect of intracellular species on these important markers of DKD progression.

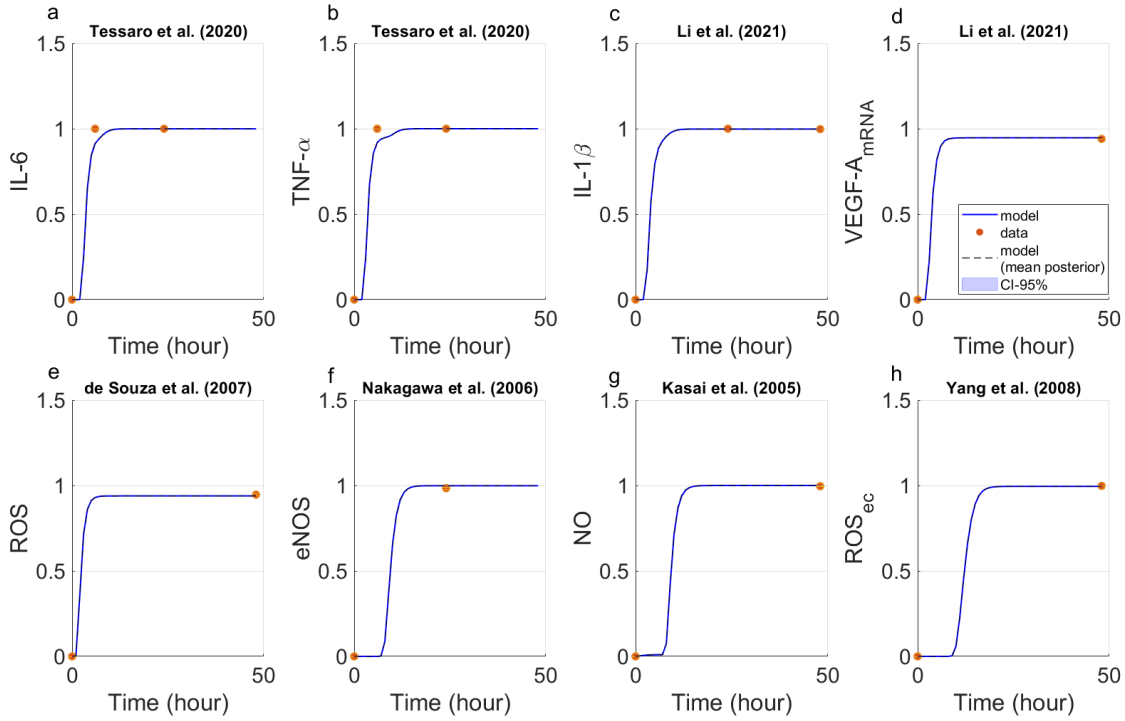

Figure 5: Network model fitted to biochemical data from (9, 13, 62, 63, 65, 67) upon stimulation with lipopolysaccharide (LPS) for 48 hours ($W_{\mathrm{GLU}} = 0$ and $W_{\mathrm{LPS}} = 1$). A semi-quantitative comparison of optimal model response against normalized protein levels of (a) IL-6, (b) TNF-α, (c) IL-1β, (d) VEGF-A (mRNA) levels, (e) ROS fluorescence, (f) eNOS, (g) NO, and (h) $\mathrm{ROS_{ec}}$. The optimal model prediction is shown as a blue solid line, mean prediction is shown as a dashed line, data are shown as orange points, and the 95% confidence region is shown as a blue-shaded region. Species activity above half-maximal activity (0.5) denotes relative upregulation, and species activity below half-maximal activity (0.5) denotes relative downregulation. The subscript "ec" denotes intracellular expression in glomerular endothelial cells. IL: interleukin. TNF: tumor necrosis factor. ROS: reactive oxygen species. VEGF: vascular endothelial growth factor. NO: nitric oxide. eNOS: endothelial nitric oxide synthase.

Upon stimulation with both GLU and LPS stimuli, the network model predicts a synergic response when both stimuli are active, as shown in Fig. 6. We calibrated the model responses such as IL-6, TNF-α, IL-1β, ROS, VEGF-A, eNOS, NO, and $\mathrm{ROS_{ec}}$ for this treatment condition. We observed that pro-inflammatory cytokines (Fig. 6a-6c) and ROS (Fig. 6e, 6h) were upregulated as also seen for other treatment conditions. VEGF-A activity was increased in macrophages after an initial delay which is possibly due to a combination of glucose-dependent downregulation and LPS-dependent upregulation of VEGF-A (Fig. 6d). Similarly, we observed that NO activity was upregulated with a slight delay, which shows the negative effect of GLU on NO and the positive effect of LPS and VEGF on NO (Fig. 6g). In our network, when both GLU and LPS stimuli were active, LPS stimulus dominated the expression of growth factors, cytokines, and ROS.

The optimized species and reaction parameters are provided in Table 1 and 2. The most sensitive reaction weight parameters (W) were optimized, rest were set to a default value of 1. A reaction weight value of 1 implies that 100% of input is available for activation or inhibition of output species. Similarly, sensitive half effect (EC_{50}) parameters were optimized, rest were set to a default value of 0.5. Any value below 1 suggests less than 100% activation or inhibition of output species. EC_{50} value below or above 0.5 indicates that less than 50% or more than 50% of input species is required to achieve maximum output activity, respectively. The initial value (y_0) has a default value of 0. The initial value (y_0) of VEGF-A (mRNA), NO, eNOS, and VEGF-A was estimated close to 1 to capture the relative downregulation effect from baseline values (Table 2).

The fitted model is validated with available *in vitro* validation dataset from multiple sources (8, 66–70, 89) that are not part of the calibration dataset. The model validation is performed across three treatment conditions: GLU only (Fig. 7), LPS

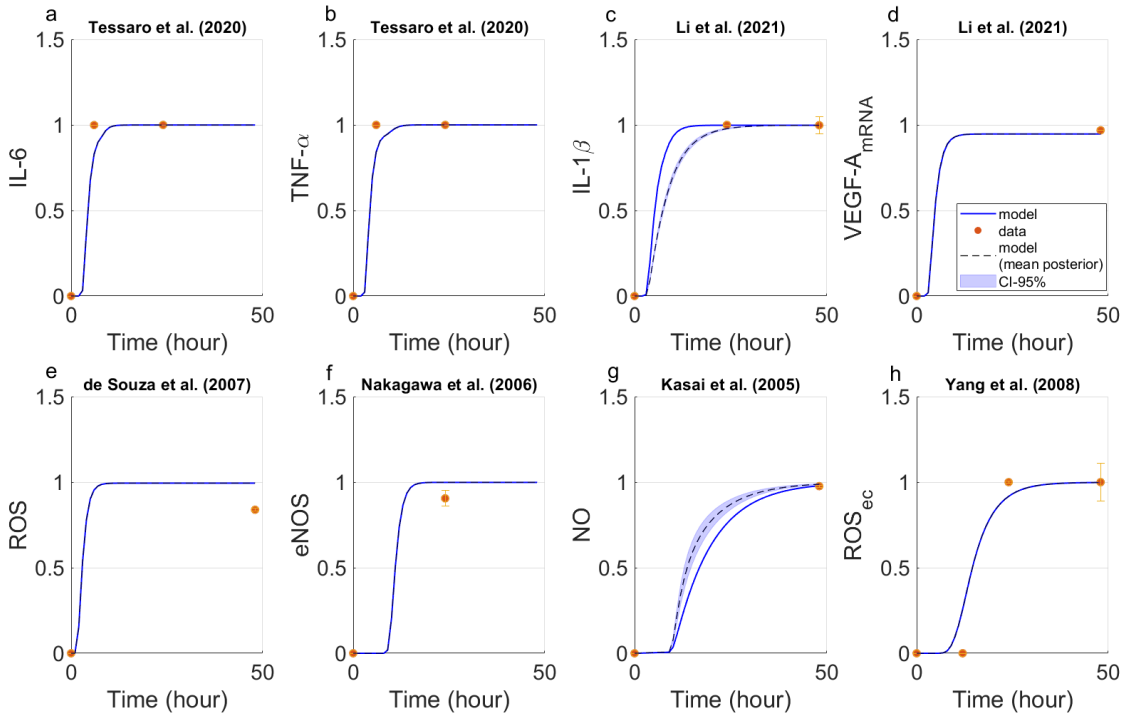

Figure 6: Network model fitted to biochemical data from (9, 13, 62, 63, 65, 67) upon stimulation with both glucose (GLU) and lipopolysaccharide (LPS) for 48 hours ($W_{\mathrm{GLU}} = 1$ and $W_{\mathrm{LPS}} = 1$). A semi-quantitative comparison of optimal model response against normalized protein levels of (a) IL-6, (b) TNF-α, (c) IL-1β, (d) VEGF-A (mRNA) levels, (e) ROS fluorescence, (f) eNOS, (g) NO, and (h) $\mathrm{ROS_{ec}}$. The optimal model prediction is shown as a blue solid line, mean prediction is shown as a dashed line, data are shown as orange points, and the 95% confidence region is shown as a blue-shaded region. Species activity above half-maximal activity (0.5) denotes relative upregulation, and species activity below half-maximal activity (0.5) denotes relative downregulation. The subscript "ec" denotes intracellular expression in glomerular endothelial cells. IL: interleukin. TNF: tumor necrosis factor. ROS: reactive oxygen species. VEGF: vascular endothelial growth factor. NO: nitric oxide. eNOS: endothelial nitric oxide synthase.

Table 1: List of optimal reaction parameters for the model. Reaction weight (W), Hill coefficient (n), and half-maximal effect (EC_{50}) are shown for respective reaction rules or interactions. Reaction rule $A\&B \Rightarrow C$ denotes the AND logic operator between input A and input B to give output C. Reaction rule $A \Rightarrow C$ denotes input A gives output C. Default values of W, n, and EC_{50} are 1, 1.4, and 0.5, respectively. $W = 0$ for $\Rightarrow$ GLU and $\Rightarrow$ LPS reaction rules represent inactive states, whereas $W = 1$ represents fully active states.

Index	**Reaction Rule**	W	n	EC_{50}
1	$\Rightarrow$ GLU	1.00	1.40	0.50
2	$\Rightarrow$ LPS	0.00	1.40	0.50
3	LPS $\Rightarrow$ TLR4	1.00	2.73	0.44
4	GLU $\Rightarrow$ AGE	1.00	1.40	0.50
5	AGE $\Rightarrow$ RAGE	1.00	2.70	0.50
6	RAGE $\Rightarrow$ NADPH	0.94	2.47	0.52
7	TLR4 & ROS $\Rightarrow$ NFκB	1.00	2.72	0.50
8	TLR4 $\Rightarrow$ PI3K	0.95	2.67	0.42
9	NADPH $\Rightarrow$ ROS	0.95	2.62	0.56
10	PI3K $\Rightarrow$ AKT	1.00	2.67	0.50
11	PI3K $\Rightarrow$ ROS	0.95	2.69	0.37
12	NFκB$_{ec}$ $\Rightarrow$ TNF-α	1.00	4.00	0.84
13	AKT $\Rightarrow$ NFκB	1.00	2.69	0.50
14	NFκB $\Rightarrow$ IL-6	0.95	2.41	0.42
15	NFκB $\Rightarrow$ TNF-α	0.95	2.99	0.42
16	NFκB $\Rightarrow$ VEGF-A$_{mRNA}$	0.95	2.73	0.42
17	VEGF-A$_{mRNA}$ $\Rightarrow$ VEGF-A	0.95	2.76	0.63
18	NFκB $\Rightarrow$ IL-1β	0.95	2.99	0.47
19	VEGF-A $\Rightarrow$ VEGFR1	1.00	2.73	0.50
20	VEGF-A $\Rightarrow$ VEGFR2	1.00	2.72	0.50
21	AGE $\Rightarrow$ RAGE$_{ec}$	1.00	1.41	0.84
22	RAGE$_{ec}$ $\Rightarrow$ NADPH$_{ec}$	0.94	1.41	0.84
23	VEGFR2 $\Rightarrow$ PI3K$_{ec}$	1.00	2.84	0.50
24	VEGFR1 $\Rightarrow$ PI3K$_{ec}$	1.00	2.73	0.50
25	NADPH$_{ec}$ $\Rightarrow$ ROS$_{ec}$	0.95	4.00	0.84
26	PI3K$_{ec}$ $\Rightarrow$ AKT$_{ec}$	1.00	2.93	0.75
27	AKT$_{ec}$ $\Rightarrow$ eNOS	1.00	3.17	0.57
28	VEGFR1 $\Rightarrow$ PLC-γ	1.00	1.40	0.50
29	PLC-γ $\Rightarrow$ NFκB$_{ec}$	1.00	1.40	0.50
30	ROS$_{ec}$ $\Rightarrow$ NFκB$_{ec}$	1.00	2.73	0.01
31	NFκB$_{ec}$ $\Rightarrow$ IL-6	0.99	3.00	0.43
32	NFκB$_{ec}$ $\Rightarrow$ IL-1β	0.96	2.63	0.44
33	eNOS $\Rightarrow$ NO	1.00	1.40	0.16
34	eNOS $\Rightarrow$ ROS$_{ec}$	1.00	3.98	0.84
35	ROS$_{ec}$ & NO $\Rightarrow$ ONOO	1.00	1.40	0.50
36	!NO $\Rightarrow$ Ca	1.00	2.69	0.50
37	PLC-γ $\Rightarrow$ Ca	1.00	1.40	0.50
38	Ca $\Rightarrow$ pJunction	1.00	1.40	0.50
39	pJunction $\Rightarrow$ Gap Width	1.00	1.40	0.50
40	Ca $\Rightarrow$ NO	0.01	1.40	0.50

Table 2: List of optimal species parameters for the model species. The time constant (τ) and initial value (y_0) for individual species used in the model are shown for each treatment condition. The default value of τ is 1 hour, the default value of y_0 is 0, and the default value of y_{max} is 1 for all species. $y_0 = 1$ indicates that initial value was set to 1 when relative downregulation from baseline was observed.

		GLU only		**LPS only**		**GLU and LPS**	
Index	**Species**	τ	y_0	τ	y_0	τ	y_0
1	GLU	1	0	1	0	1	0
2	LPS	5.2	0	0.8	0	1	0
3	AGE	1	0	1	0	1	0
4	VEGFR1	1	0	1	0	1	0
5	VEGFR2	1	0	1	0	1	0
6	VEGF-A_{mRNA}	3.1	1	0.97	0	1.52	0
7	$RAGE_{ec}$	1	0	1	0	1	0
8	RAGE	1	0	1	0	1	0
9	TLR4	5.1	0	0.8	0	1	0
10	NADPH	1	0	1	0	1	0
11	$NADPH_{ec}$	1	0	1	0	1	0
12	ROS_{ec}	10.0	0	1.15	0	5.15	0
13	ROS	5.9	0	0.8	0	1.00	0
14	PI3K	4.9	0	0.8	0	1	0
15	AKT	1	0	1	0	1	0
16	$PI3K_{ec}$	6.5	0	0.87	0	1.00	0
17	AKT_{ec}	6.1	0	0.83	0	1.00	0
18	$NF\kappa B_{ec}$	1	0	1	0	1	0
19	NFκB	5.4	0	0.8	0	1	0
20	NO	4.4	1	0.80	0	9.84	0
21	ONOO	1	0	1	0	1	0
22	eNOS	1.9	1	0.95	0	1.00	0
23	IL-6	4.8	0	0.8	0	1	0
24	TNF-α	10.0	0	0.8	0	1	0
25	IL-1β	6.2	0	1.15	0	1.98	0
26	PLC-γ	1	0	1	0	1	0
27	VEGF-A	3.4	1	1.08	0	1.06	0
28	pJunction	1	0	1	0	1	0
29	Ca	1	0	1	0	1	0
30	Gap Width	1	0	1	0	1	0

only (Fig. 8), and both GLU and LPS (Fig. 9). The fitted model simulations agree with available validation data for TNF-α, IL-6, IL-1β, ROS, VEGF-A, eNOS, NO, and ROS_{ec}. The change in GEC fenestration width in our network depends on the phosphorylation of cell-cell junction proteins such as VE-cadherin, which is responsible for opening or closing of the cell-cell junctions. We validated the expression of VE-cadherin levels upon stimulation with LPS stimulus (Fig. 8) Limited published studies report glomerular endothelial fenestration width in the diabetic state. However, we were able to qualitatively show the effect of dysregulated signaling and species expression on fenestration width (Fig. 12). These short-term model simulations contribute to our understanding of dysregulated signaling interactions between macrophages and GECs. Despite a short-term exposure of 48 hours to glucose and LPS, these cells undergo significant perturbations in signaling pathways and species expression. Hence, a deeper understanding of signaling dysregulation in the early stage of DKD can guide us to a mechanistic link between diabetes-mediated immune response and cellular dysfunction in GECs.

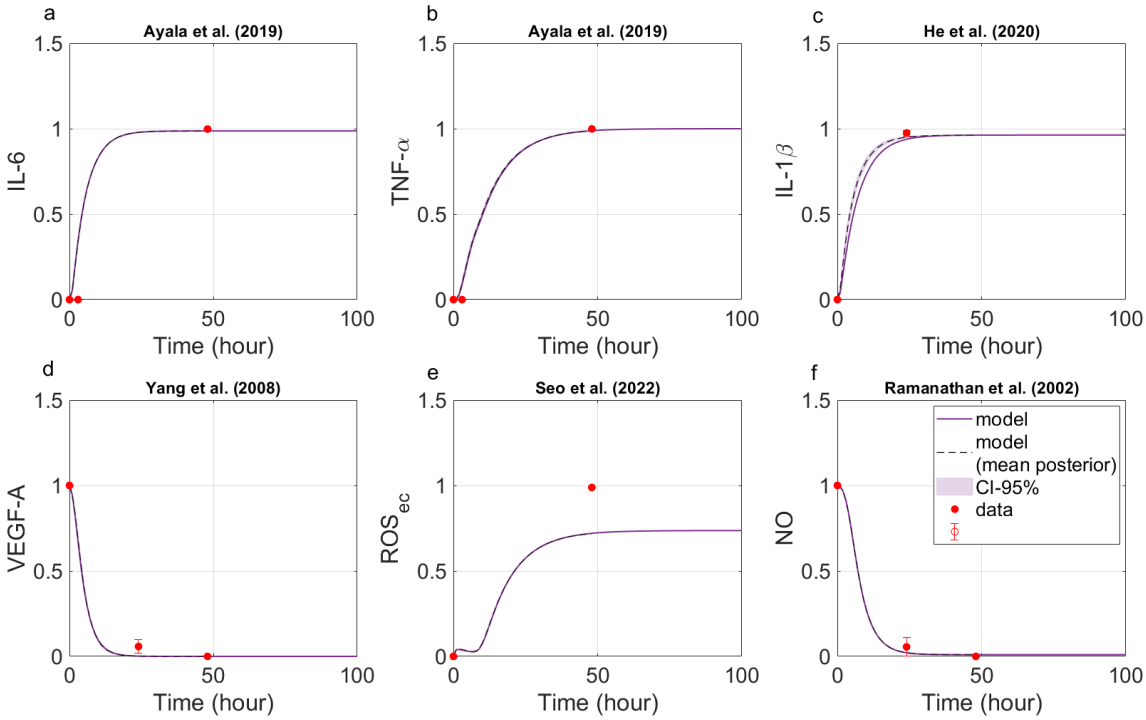

Figure 7: Network responses are validated with biochemical data available from cell culture experiments (8, 66–69) upon stimulation with glucose (GLU) for 48 hours ($W_{GLU} = 1$ and $W_{LPS} = 0$). Model validation of selected species against available normalized protein levels of (a) IL-6, (b) TNF-α, (c) IL-1β protein levels, (d) VEGF-A levels, (e) ROS_{ec}, and (f) NO. The optimal model prediction is shown as a purple solid line, the mean prediction is shown as a dashed line, validation data are shown as orange points, and the 95% confidence region is shown as a purple-shaded region. Species activity above half-maximal activity (0.5) denotes relative upregulation, and species activity below half-maximal activity (0.5) denotes relative downregulation. The subscript "ec" denotes intracellular expression in glomerular endothelial cells. IL: interleukin. TNF: tumor necrosis factor. ROS: reactive oxygen species. VEGF: vascular endothelial growth factor. NO: nitric oxide.

Analysis of protein signaling network

Through our network, we demonstrated the effect of hyperglycemia on cell signaling pathways, cellular micro-environment, and resulting perturbations in both macrophages and GECs. We demonstrated that significantly high levels of GLU and LPS affect macrophage phenotype and activate GECs. The model captured this change in phenotype in macrophages with an increased expression of pro-inflammatory species such as IL-6, TNF-α, IL-1β, and ROS by both macrophages and GECs. These pro-inflammatory species affect macrophage phenotype through autocrine or paracrine signaling (90). The consistent secretion of these inflammatory molecules and ongoing inflammation leads to a chronic shift in macrophage phenotype (90). Although not all such autocrine or paracrine signaling interactions were included in our network, we depicted this effect on macrophages through ROS-mediated PI3K signaling and VEGF-mediated VEGF receptor activation. In our network (Fig. 1), an

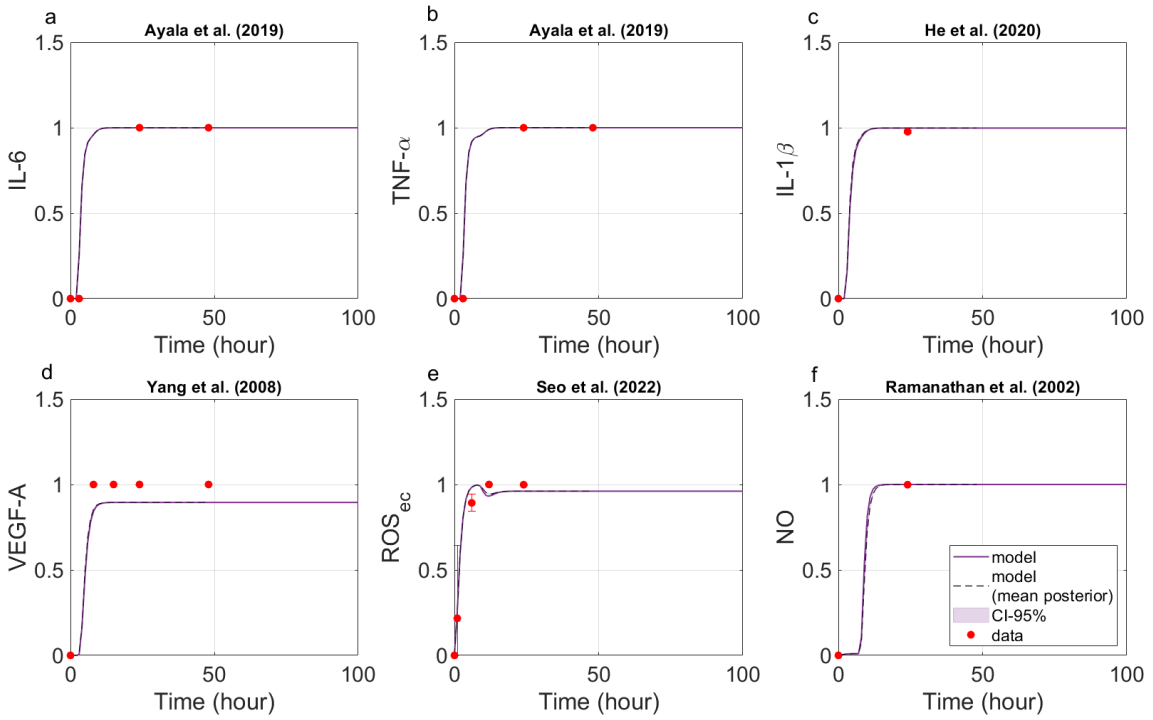

Figure 8: Network responses are validated with biochemical data available from cell culture experiments (8, 66, 67, 69, 70) upon stimulation with lipopolysaccharide (LPS) for 48 hours ($W_{\mathrm{GLU}} = 0$ and $W_{\mathrm{LPS}} = 1$). Model validation of selected species against available normalized protein levels of (a) IL-6, (b) TNF-α, (c) IL-1β protein levels, (d) VEGF-A levels, (e) phosphorylated VE-cadherin, and (f) NO. VE-cadherin represents the pJunction node in the network. The optimal model prediction is shown as a purple solid line, the mean prediction is shown as a dashed line, validation data are shown as orange points, and the 95% confidence region is shown as a purple-shaded region. The subscript "ec" denotes intracellular expression in glomerular endothelial cells. IL: interleukin. TNF: tumor necrosis factor. VEGF: vascular endothelial growth factor. NO: nitric oxide.

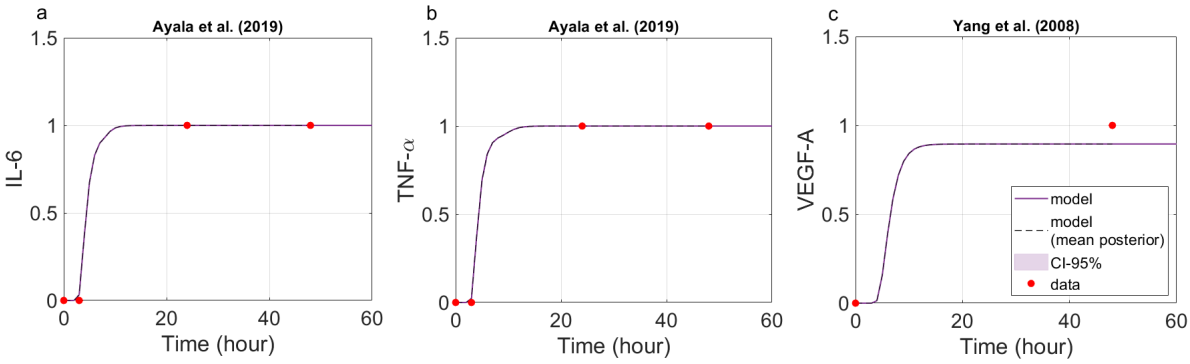

Figure 9: Network responses are validated with biochemical data available from cell culture experiments (8, 67) upon stimulation with both glucose (GLU) and lipopolysaccharide (LPS) for 48 hours ($W_{\mathrm{GLU}} = 1$ and $W_{\mathrm{LPS}} = 1$). Model validation of selected species against available normalized protein levels of (a) IL-6, (b) TNF-α, and (c) VEGF-A. The optimal model prediction is shown as a purple solid line, the mean prediction is shown as a dashed line, validation data are shown as orange points, and the 95% confidence region is shown as a purple-shaded region. IL: interleukin. TNF: tumor necrosis factor. VEGF: vascular endothelial growth factor.

over-expression of intracellular ROS activity in the macrophages is preliminary to causing disturbance to downstream signaling (Fig. 4e, 5e). As ROS is activated via multiple routes by either stimulus, it is a relevant link that should be explored to target dysregulated downstream pathways.

Co-culture experimental studies showed that elevated GLU levels without a pro-inflammatory stimulus could not significantly upregulate cytokine or VEGF-A expression (13). In our network, an *AND* logical rule between LPS-stimulated PI3K signaling and glucose-stimulated ROS signaling ensured that pro-inflammatory species cannot be activated without LPS. Active VEGF-A selectively binds to its receptors VEGFR1 and VEGFR2 on GECs. The lower kinase activity of VEGFR1 and higher affinity to VEGF-A affect its downstream response to PI3K-AKT kinases. VEGFR1 also promotes downstream pro-inflammatory signaling via the PLC-γ pathway. As a result of the competitive binding of VEGF-A to its receptors, the cellular response and behavior of the activated GECs were affected. The resulting perturbations involved insufficient activation of VEGF-mediated PI3K-AKT signaling, reduced NO bioavailability due to uncoupling of endothelial NO, increased pro-inflammatory cytokines expression, and macrophage infiltration. These observations suggest that targeting this competitive receptor activation by VEGF-A could be helpful in modulating signaling dysregulation in GECs.

Our model showed the effect of VEGF-dependent signaling and NO bioavailability on junction protein phosphorylation. From a molecular standpoint, the endothelial barrier is sealed by cell-cell junction proteins, among which VE-cadherin serves as a cornerstone. The endothelial barrier is maintained by VE-cadherin and associated catenins in a non-phosphorylated state (61). The modulated phosphorylation of these junction proteins allows for the selective opening or closing of the barrier. The relationship between VEGF-dependent NO and phosphorylated junction proteins was captured as a negative feedback loop in the network. Using a negative feedback loop between NO and Ca allowed for better information processing and cell behavior regulation in our network. Lower than healthy NO levels in GECs affected barrier integrity reversibly (31). We showed that hyperglycemic conditions caused a prolonged and consistent disruption of the GEC barrier integrity. Ultimately, this reduced cell-cell junction integrity widens the intercellular gaps between GECs. Therefore, targeting this mechanistic pathway that links NO and GEC junction integrity is relevant to mitigate glomerular endothelial dysfunction.

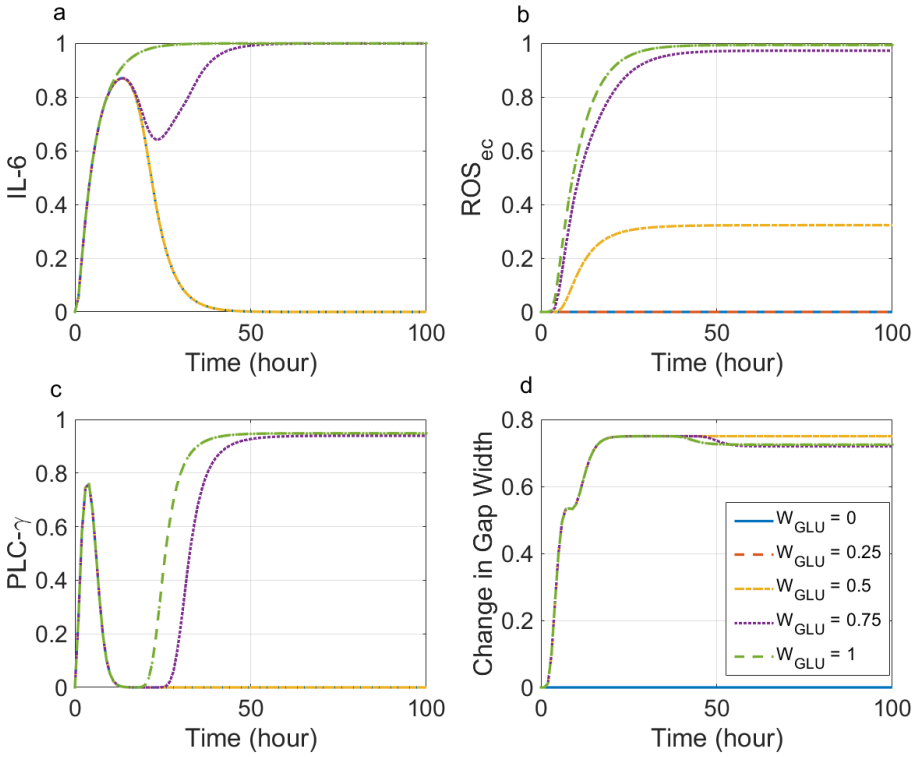

Figure 10: Model predictions upon stimulation with partially active glucose (GLU) stimulus to mimic the increase in glucose levels in the early stage of diabetes. W_{GLU} varied between 0.25 to 1. W_{LPS} is set to 0 to mimic a non-inflammatory state. The above prediction is qualitative and suggests the change in protein expression from baseline. IL: interleukin. ROS: reactive oxygen species. PLC: phospholipase C.

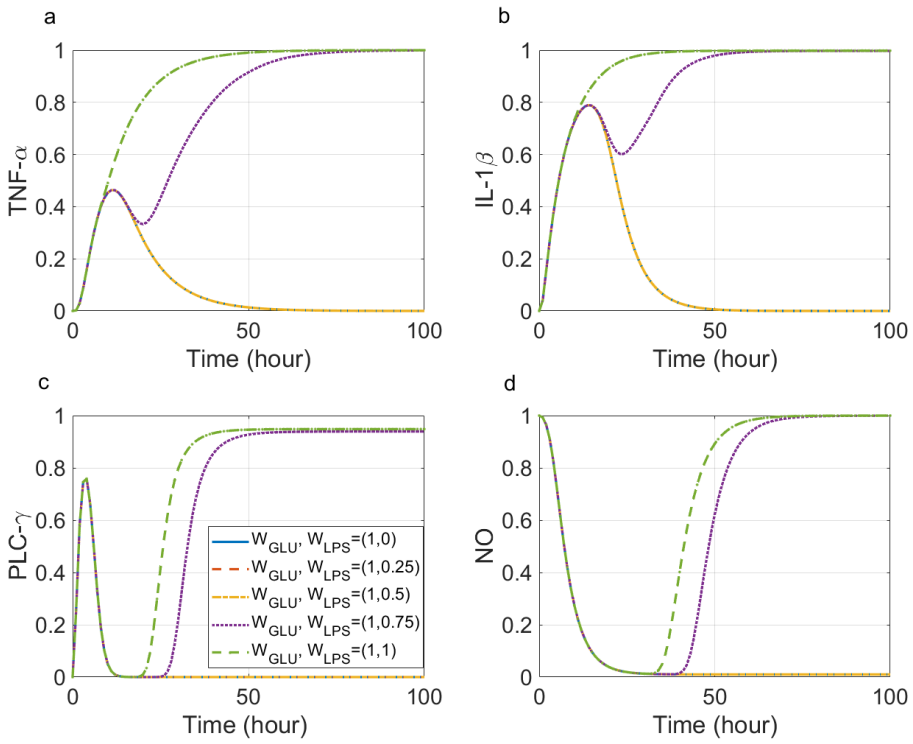

Figure 11: Model predictions upon stimulation with partially active lipopolysaccharide (LPS) and fully active glucose (GLU) stimulus ($W_{\mathrm{GLU}} = 1$) to mimic gradual rise in inflammation in the early-stage of diabetic kidney disease (DKD). W_{LPS} was varied between 0 and 1. The above prediction is qualitative and suggests the change in protein expression from baseline. The choice of initial values (0 or 1) was subject to upregulation or downregulation from baseline values (in a healthy state). IL: interleukin. ROS: reactive oxygen species. PLC: phospholipase C. NO: nitric oxide.

The validated network model can be used to make insightful predictions under different combinations of stimuli treatments. The model simulations shown previously were performed in the presence of fully active stimuli. We also predicted network responses under partially active stimuli. To study the potency of GLU and LPS stimuli, we varied the reaction weight (W) for GLU and LPS. We observed that 50% of the maximum glucose activity ($W_{\mathrm{GLU}} > 0.5$) was sufficient to activate and express IL-6 cytokine (Fig. 10a). However, prolonged exposure to low glucose activity was insufficient to sustain IL-6 levels, and IL-6 activity returned to the baseline. The intracellular levels of ROS were lower in macrophages when stimulated with low glucose levels (below 0.5) (Fig. 10b). We also observed a reduced expression of PLC-γ protein in the presence of low glucose levels and the absence of LPS stimulus (Fig. 10c). As previously observed, high glucose downregulated VEGF-A activity, which can explain lowered PLC-γ activity (Fig. 10c). Increasing glucose levels cause a full activation of the PLC-γ signaling protein. We observed no recovery in the GEC gap width when exposed to low to high glucose levels ($0.25 < W_{\mathrm{GLU}} < 1$) (Fig. 10d). We believe further analysis is needed to identify signaling interactions and molecules responsible for the change in GEC gap width. The macrophages and glomerular endothelial cells were also stimulated with varying levels of LPS when glucose levels were high (Fig. 11). This condition mimics the early phase of DKD development, where high glucose levels cause metabolic dysregulation in pro-inflammatory species and the environment. Increasing levels of LPS activity had a substantial effect on the over-expression of the pro-inflammatory cytokines, TNF-α and IL-1β, and PLC-γ activity (Fig. 11a, b, c). We also observed that glucose-dependent downregulation of NO activity recovered to baseline level as LPS activity increased (Fig. 11d). A quarter of maximum LPS activity was sufficient to recover downregulated NO levels. LPS stimulus regulates VEGF-A expression in macrophages, which restored NO levels to baseline.

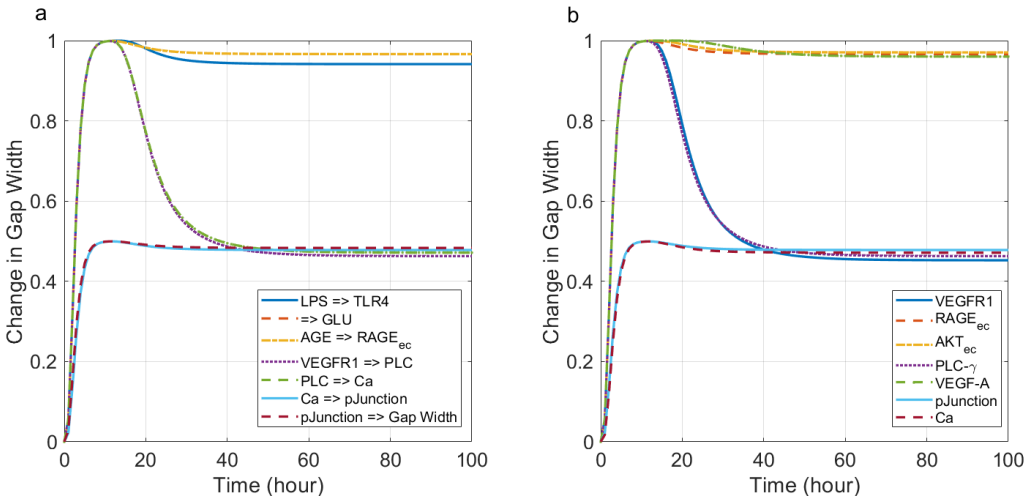

Figure 12: (a) The influence of interactions on the fractional change in GEC Gap Width. The reaction weight W of each interaction (left) was reduced by 50% from its original value. (b) The effect of partial knockdown of sensitive species on the fractional change in GEC Gap Width. $y_{\max}$ of the sensitive species (right) was reduced by 50% from its original value. TLR: toll-like receptor. AGE: advanced glycation end product. RAGE: receptor of advanced glycation end product. NADPH: nicotinamide adenine dinucleotide phosphate. NFκB: nuclear factor kappa B. VEGF: vascular endothelial growth factor. VEGFR: vascular endothelial growth factor receptor. PLC: phospholipase C. Ca: calcium.

We also identified influential pathways from our network model, which trigger inflammation, and GEC activation and dysfunction in the early stage of DKD. We analyzed the reaction weight (W) of all interactions and $y_{\max}$ parameter of all species in the network. The reaction weight (W) modulates the strength or intensity of the reactions in the network. $y_{\max}$ modulates the maximum activation of species in the network. We performed a local sensitivity analysis on the LBODE model. We perturbed the W (Fig. A9) and $y_{\max}$ (Fig. A10) were perturbed by 15% below their optimal value. $y_{\max}$ below or above 1 denotes the knockdown or overexpression of a species in the network, respectively. Among the most sensitive reactions, we found that LPS $\Rightarrow$ TLR4, $\Rightarrow$ GLU, AGE $\Rightarrow$ RAGE$_{ec}$, VEGFR1 $\Rightarrow$ PLC, PLC $\Rightarrow$ Ca, Ca $\Rightarrow$ pJunction, pJunc $\Rightarrow$ Gap Width were reactions that had the most effect on the GEC Gap Width (Fig. 12a). We targeted the most influential interactions and species in the network. VEGFR1, RAGE$_{ec}$, AKT$_{ec}$, PLC-γ, VEGF-A, pJunction, and Ca affect the GEC Gap Width significantly (Fig. 12b). Our predictive findings suggest that a multi-targeted approach is necessary to modulate the changes in GEC fenestration size observed in the early stage of DKD development and progression. The influential species and interactions identified by our model can be further analyzed in detail through computational modeling and/or experimental studies.

CONCLUSIONS

In this study, we presented a multi-cell LBODEs model to understand the role of diabetes and immune response in the progression of microvascular complications in the diabetic kidney. We created a signaling network of crosstalk between macrophages and GECs stimulated by two inputs, high GLU and LPS, a pro-inflammatory stimulus. The signaling network was modeled using continuous ODEs and logic-based interaction rules, where interaction between species was formulated using normalized-Hill functions. The model was fitted and validated against published data from *in vitro* experiments performed on murine macrophage cell lines and endothelial cell lines. Our modeling approach combines the advantages of quantitative biochemical models and qualitative LBMs. These pathways and interactions between macrophages and GECs in the early stage of DKD have not been computationally studied before. Our model also incorporated the effect of competitive activation of VEGF receptors in activated GECs, which has not been shown in the context of DKD progression previously. In the presence of high GLU and a pro-inflammatory stimulus like LPS, we observed upregulation of normalized protein values of pro-inflammatory cytokines (IL-6, TNF-α, and IL-1β), oxidative stress, VEGF-A, and GEC fenestration width. We found that oxidative stress in macrophages significantly affected interconnected species, NFκB transcription factor, and NO bioavailability in the downstream signaling response. Our results contribute to understanding the role of signaling and molecular perturbations on macrophage-dependent inflammation and GEC morphology. We found that partial knockdown of VEGFR1, PLC-γ, pJunction, and Ca partially recovered the GEC fenestration size. The VEGFR1/PLC-γ/Calicum signaling axis modulates the GEC fenestration size significantly. Through our signaling network, we have studied glucose-mediated inflammatory pathways in the diabetic kidney, contributing to a comprehensive understanding of DKD development and progression. These identified interactions can be further analyzed individually through modeling or experimentation. Our predictive findings indicate that a multi-targeted approach is necessary to modulate the early markers of DKD development and progression.

APPENDIX

Model equations

The following model equations govern network interactions.

$$\frac{d\text{GLU}}{dt} = \frac{y_{\text{max}_{\text{GLU}}} W_{\text{GLU}} - \text{GLU}}{\tau_{\text{GLU}}} \tag{A1}$$

$$\frac{d\text{LPS}}{dt} = \frac{y_{\text{max}_{\text{LPS}}} W_{\text{LPS}} - \text{LPS}}{\tau_{\text{LPS}}} \tag{A2}$$

$$\frac{d\text{AGE}}{dt} = \frac{y_{\text{max}_{\text{AGE}}} f_{\text{act}}(\text{GLU}) - \text{AGE}}{\tau_{\text{AGE}}} \tag{A3}$$

$$\frac{d\text{VEGFR1}}{dt} = \frac{y_{\text{max}_{\text{VEGFR1}}} f_{\text{act}}(\text{VEGF-A}) - \text{VEGFR1}}{\tau_{\text{VEGFR1}}} \tag{A4}$$

$$\frac{d\text{VEGFR2}}{dt} = \frac{y_{\text{max}_{\text{VEGFR2}}} f_{\text{act}}(\text{VEGF-A}) - \text{VEGFR2}}{\tau_{\text{VEGFR2}}} \tag{A5}$$

$$\frac{d\text{VEGF-A}_{\text{mRNA}}}{dt} = \frac{y_{\text{max}_{\text{VEGF-A}_{\text{mRNA}}}} f_{\text{act}}(\text{NF}\kappa\text{B}) - \text{VEGF-A}_{\text{mRNA}}}{\tau_{\text{VEGF-A}_{\text{mRNA}}}} \tag{A6}$$

$$\frac{d\text{RAGE}}{dt} = \frac{y_{\text{max}_{\text{RAGE}}} f_{\text{act}}(\text{AGE}) - \text{RAGE}}{\tau_{\text{RAGE}}} \tag{A7}$$

$$\frac{d\text{RAGE}_{\text{ec}}}{dt} = \frac{y_{\text{max}_{\text{RAGE}_{\text{ec}}}} f_{\text{act}}(\text{AGE}) - \text{RAGE}_{\text{ec}}}{\tau_{\text{RAGE}_{\text{ec}}}} \tag{A8}$$

$$\frac{d\text{TLR4}}{dt} = \frac{y_{\text{max}_{\text{TLR4}}} f_{\text{act}}(\text{LPS}) - \text{TLR4}}{\tau_{\text{TLR4}}} \tag{A9}$$

$$\frac{d\text{NADPH}}{dt} = \frac{y_{\text{max}_{\text{NADPH}}} f_{\text{act}}(\text{RAGE}) - \text{NADPH}}{\tau_{\text{NADPH}}} \tag{A10}$$

$$\frac{d\text{NADPH}_{\text{ec}}}{dt} = \frac{y_{\text{max}_{\text{NADPH}_{\text{ec}}}} f_{\text{act}}(\text{RAGE}_{\text{ec}}) - \text{NADPH}_{\text{ec}}}{\tau_{\text{NADPH}_{\text{ec}}}} \tag{A11}$$

$$\frac{d\text{ROS}}{dt} = \frac{y_{\text{max}_{\text{ROS}}} OR\left(f_{\text{act}}(\text{PI3K}), f_{\text{act}}(\text{NADPH})\right) - \text{ROS}}{\tau_{\text{ROS}}} \tag{A12}$$

$$\frac{d\text{ROS}_{\text{ec}}}{dt} = \frac{y_{\text{max}_{\text{ROS}_{\text{ec}}}} OR(f_{\text{act}}(\text{eNOS}), f_{\text{act}}(\text{NADPH}_{\text{ec}})) - \text{ROS}_{\text{ec}}}{\tau_{\text{ROS}_{\text{ec}}}} \tag{A13}$$

$$\frac{d\text{PI3K}}{dt} = \frac{y_{\text{max}_{\text{PI3K}}} f_{\text{act}}(\text{TLR4}) - \text{PI3K}}{\tau_{\text{PI3K}}} \tag{A14}$$

$$\frac{d\text{AKT}}{dt} = \frac{y_{\text{max}_{\text{AKT}}} f_{\text{act}}(\text{PI3K}) - \text{AKT}}{\tau_{\text{AKT}}} \tag{A15}$$

$$\frac{d\text{PI3K}_{\text{ec}}}{dt} = \frac{y_{\text{max}_{\text{PI3K}_{\text{ec}}}} OR(f_{\text{act}}(\text{VEGFR1}), f_{\text{act}}(\text{VEGFR2})) - \text{PI3K}_{\text{ec}}}{\tau_{\text{PI3K}_{\text{ec}}}} \tag{A16}$$

$$\frac{d\text{AKT}_{\text{ec}}}{dt} = \frac{y_{\text{max}_{\text{AKT}_{\text{ec}}}} f_{\text{act}}(\text{AKT}_{\text{ec}}) - \text{AKT}_{\text{ec}}}{\tau_{\text{AKT}_{\text{ec}}}} \tag{A17}$$

$$\frac{d\text{NF}\kappa\text{B}}{dt} = \frac{y_{\text{max}_{\text{NF}\kappa\text{B}}} OR(AND(f_{\text{act}}(\text{TLR4}), f_{\text{act}}(\text{ROS})), f_{\text{act}}(\text{AKT})) - \text{NF}\kappa\text{B}}{\tau_{\text{NF}\kappa\text{B}}} \tag{A18}$$

$$\frac{d\text{NF}\kappa\text{B}_{\text{ec}}}{dt} = \frac{y_{\text{max}_{\text{NF}\kappa\text{B}_{\text{ec}}}} OR(f_{\text{act}}(\text{PLC-}\gamma), f_{\text{act}}(\text{ROS}_{\text{ec}})) - \text{NF}\kappa\text{B}_{\text{ec}}}{\tau_{\text{NF}\kappa\text{B}_{\text{ec}}}} \tag{A19}$$

$$\frac{d\text{NO}}{dt} = \frac{y_{\text{max}_{\text{NO}}} OR(f_{\text{act}}(\text{eNOS}), f_{\text{act}}(\text{Ca})) - \text{NO}}{\tau_{\text{NO}}} \tag{A20}$$

$$\frac{d\text{ONOO}}{dt} = \frac{y_{\text{max}_{\text{ONOO}}} AND(f_{\text{act}}(\text{NO}), f_{\text{act}}(\text{ROS}_{\text{ec}})) - \text{ONOO}}{\tau_{\text{ONOO}}} \tag{A21}$$

$$\frac{d\text{eNOS}}{dt} = \frac{y_{\text{max}_{\text{eNOS}}} f_{\text{act}}(\text{AKT}_{\text{ec}}) - \text{eNOS}}{\tau_{\text{eNOS}}} \tag{A22}$$

$$\frac{d\text{IL-6}}{dt} = \frac{y_{\text{max}_{\text{IL-6}}} OR(f_{\text{act}}(\text{NF}\kappa\text{B}), f_{\text{act}}(\text{NF}\kappa\text{B}_{\text{ec}})) - \text{IL-6}}{\tau_{\text{IL-6}}} \tag{A23}$$

$$\frac{d\text{TNF-}\alpha}{dt} = \frac{y_{\text{max}_{\text{TNF-}\alpha}} OR(f_{\text{act}}(\text{NF}\kappa\text{B}), f_{\text{act}}(\text{NF}\kappa\text{B}_{\text{ec}})) - \text{TNF-}\alpha}{\tau_{\text{TNF-}\alpha}} \tag{A24}$$

$$\frac{d\text{IL-}\beta}{dt} = \frac{y_{\text{max}_{\text{IL-1}\beta}} OR(f_{\text{act}}(\text{NF}\kappa\text{B}), f_{\text{act}}(\text{NF}\kappa\text{B}_{\text{ec}})) - \text{IL-1}\beta}{\tau_{\text{IL-1}\beta}} \tag{A25}$$

$$\frac{d\text{PLC-}\gamma}{dt} = \frac{y_{\text{max}_{\text{PLC-}\gamma}} f_{\text{act}}(\text{VEGFR1}) - \text{PLC-}\gamma}{\tau_{\text{PLC-}\gamma}} \tag{A26}$$

$$\frac{d\text{VEGF-A}}{dt} = \frac{y_{\text{max}_{\text{VEGF-A}}} f_{\text{act}}(\text{VEGF-A}_{\text{mRNA}}) - \text{VEGF-A}}{\tau_{\text{VEGF-A}}} \tag{A27}$$

$$\frac{d\text{Ca}}{dt} = \frac{y_{\text{max}_{\text{Ca}}} OR(f_{\text{inhib}}(\text{NO}), f_{\text{act}}(\text{PLC-}\gamma)) - \text{Ca}}{\tau_{\text{Ca}}} \tag{A28}$$

$$\frac{d\text{pJunction}}{dt} = \frac{y_{\text{max}_{\text{pJunction}}} f_{\text{act}}(\text{Ca}) - \text{pJunction}}{\tau_{\text{pJunction}}} \tag{A29}$$

$$\frac{d\text{Gap Width}}{dt} = \frac{y_{\text{max}_{\text{Gap Width}}} f_{\text{act}}(\text{pJunction}) - \text{Gap Width}}{\tau_{\text{Gap Width}}} \tag{A30}$$

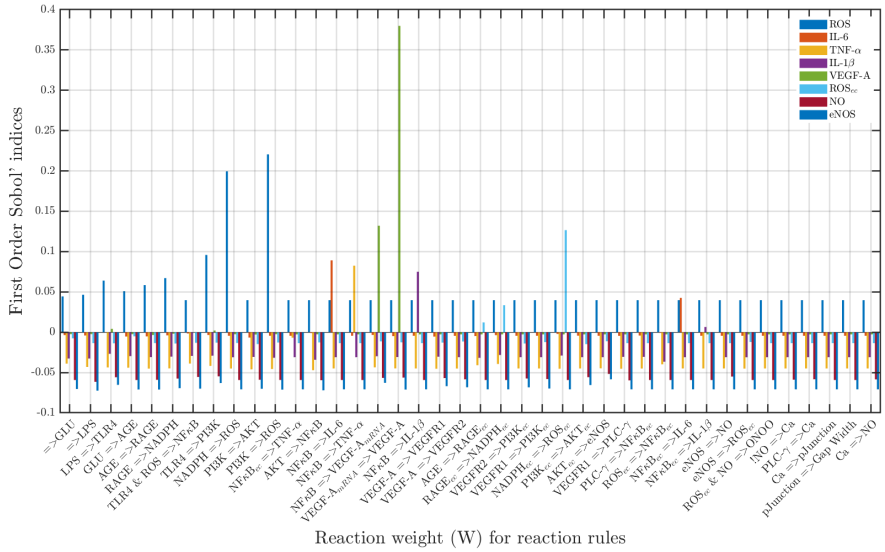

Figure A1: First order Sobol indices for reaction weight (W) for respective reaction rules. The Sobol sensitivity for each parameter was calculated against species response of ROS, IL-6, TNF-α, IL-1β, VEGF-A, ROS_{ec}, NO, and eNOS at 48 hours. These species are ordered on the plot from left to right for each W parameter.

Model parameters

The default values of species parameters τ, y_0, and $y_{\max}$ are 1, 0, and 1, respectively. The default values of reaction parameters W, n, and EC_{50} are 1, 1.4, and 0.5, respectively. Fig. A5-A8 provide the relatively sensitive parameters (W, n, EC_{50}, and τ) as obtained from the global sensitivity analysis (Sobol's method).

Regulatory species dynamics

We provide the dynamics of different regulatory species in the network that were not used in model fitting. The species dynamics capture the behavior of signaling molecules, transcription factors, and receptors for which we could not obtain experimental data. Fig. A11, A12, and A13 capture the species expression over 48 hours under GLU only, LPS only, and GLU and LPS treatment, respectively.

DATA AVAILABILITY

No primary data was generated in this study. The supporting MATLAB code, including parameter values, scripts for plotting, data, and documentation, can be accessed through an open-source GitHub repository (91).

ACKNOWLEDGMENTS

This work was supported by National Institutes of Health grant R35GM133763, National Science Foundation grant 2133411, and the University at Buffalo. We thank lab members for their thorough feedback on this manuscript.

GRANTS

DISCLOSURES

The authors have nothing to disclose.

AUTHOR CONTRIBUTIONS

REFERENCES

1. Centers for Disease Control and Prevention. National Diabetes Statistics Report; 2020. https://www.cdc.gov/

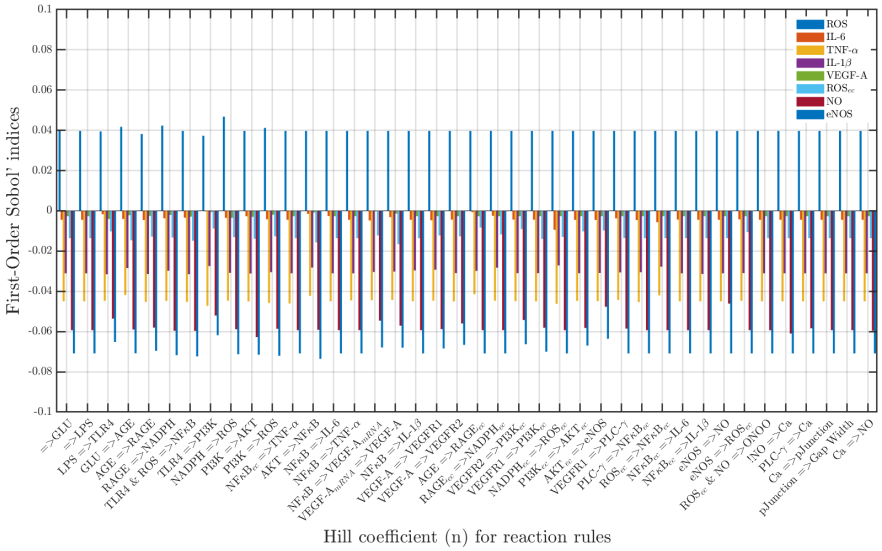

Figure A2: First order Sobol indices for Hill coefficient (n) for respective reaction rules. The Sobol sensitivity for each parameter was calculated against species response of ROS, IL-6, TNF-α, IL-1β, VEGF-A, ROS$_{ec}$, NO, and eNOS at 48 hours. These species are ordered on the plot from left to right for each n parameter.

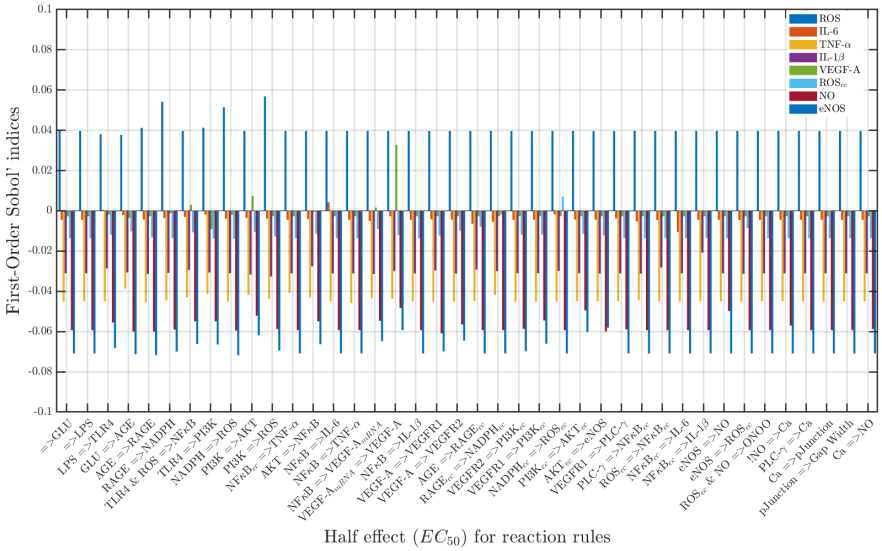

Figure A3: First order Sobol indices for half effect (EC_{50}) for respective reaction rules. The Sobol sensitivity for each parameter was calculated against species response of ROS, IL-6, TNF-α, IL-1β, VEGF-A, ROS$_{ec}$, NO, and eNOS at 48 hours. These species are ordered on the plot from left to right for each EC_{50} parameter.

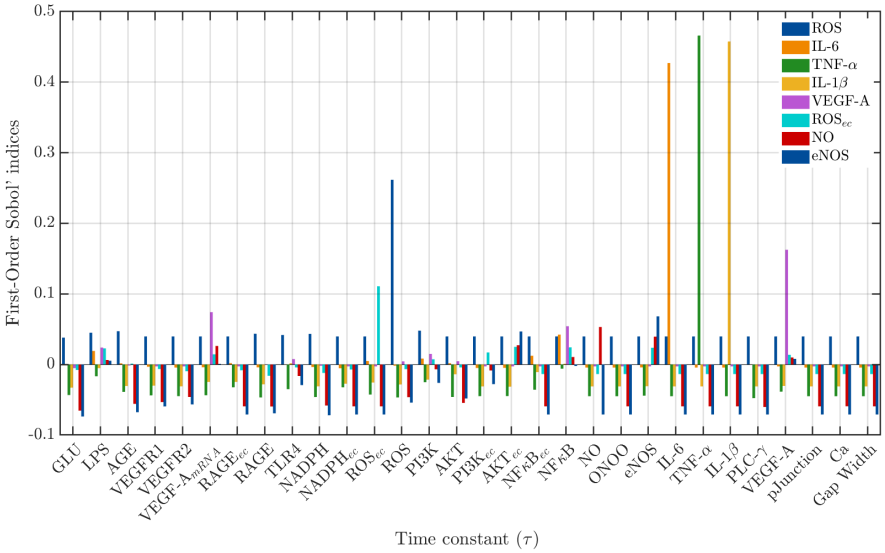

Figure A4: First order Sobol indices for time constant (τ) for respective species. The Sobol sensitivity for each parameter was calculated against species response of ROS, IL-6, TNF-α, IL-1β, VEGF-A, ROS$_ec$, NO, and eNOS at 48 hours. These species are ordered on the plot from left to right for each τ parameter.

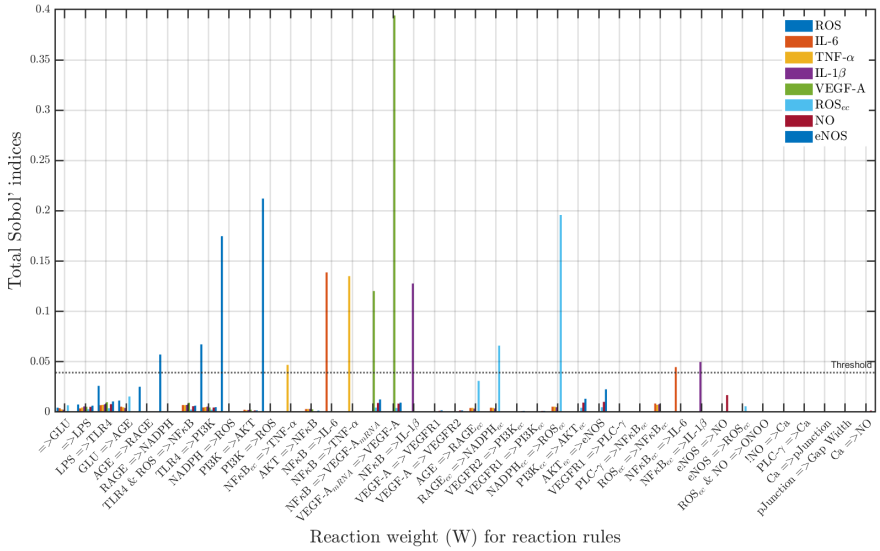

Figure A5: Total order Sobol indices for reaction weight (W) for respective reaction rules. The Sobol sensitivity for each parameter was calculated against species response of ROS, IL-6, TNF-α, IL-1β, VEGF-A, ROS$_{ec}$, NO, and eNOS at 48 hours. These species are ordered on the plot from left to right for each W parameter.

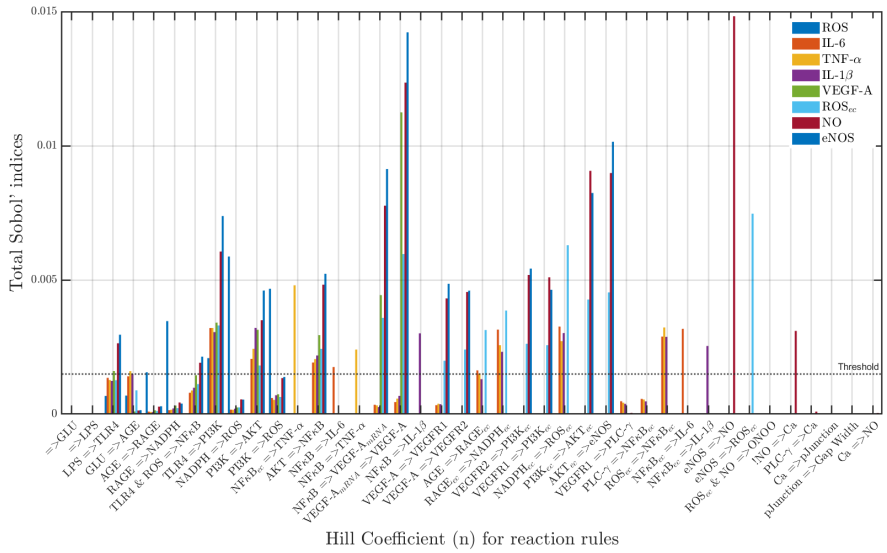

Figure A6: Total order Sobol indices for Hill coefficient (n) for respective reaction rules. The Sobol sensitivity for each parameter was calculated against species response of ROS, IL-6, TNF-α, IL-1β, VEGF-A, ROS_{ec}, NO, and eNOS at 48 hours. These species are ordered on the plot from left to right for each n parameter.

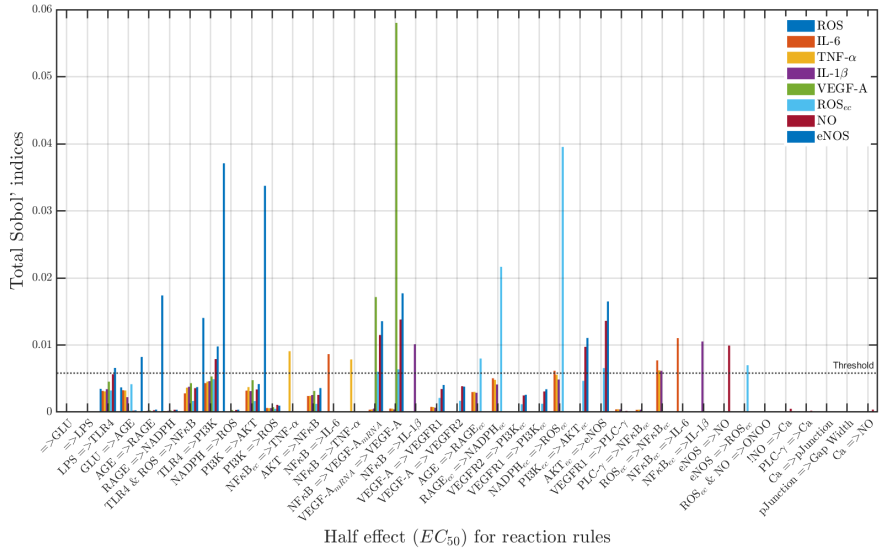

Figure A7: Total order Sobol indices for half effect (EC_{50}) for respective reaction rules. The Sobol sensitivity for each parameter was calculated against species response of ROS, IL-6, TNF-α, IL-1β, VEGF-A, ROS_{ec}, NO, and eNOS at 48 hours. These species are ordered on the plot from left to right for each EC_{50} parameter.

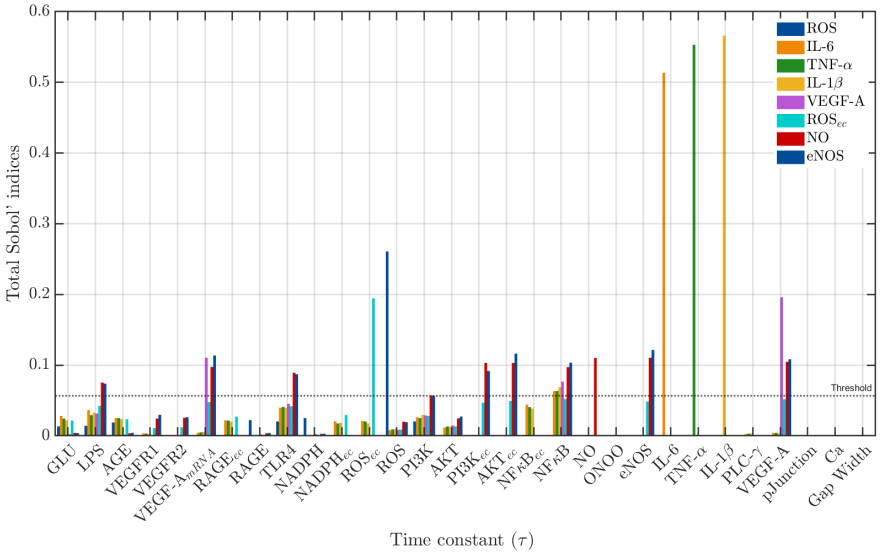

Figure A8: Total order Sobol indices for time constant (τ) for respective species. The Sobol sensitivity for each parameter was calculated against species response of ROS, IL-6, TNF-α, IL-1β, VEGF-A, ROS_{ec}, NO, and eNOS at 48 hours. These species are ordered on the plot from left to right for each τ parameter.

diabetes/data/statistics-report/index.html.

2. Yang J, Liu Z. Mechanistic pathogenesis of endothelial dysfunction in diabetic nephropathy and retinopathy. Front Endocrinol. 2022;13:816400.

3. Thomas S, Karalliedde J. Diabetic kidney disease. Medicine. 2022;50:704-10.

4. Thomas HY, Ford Versypt AN. Collagen deposition in diabetic kidney disease boosts intercellular signaling: a mathematical model. IFAC PapersOnLine. 2022;55:68-73.

5. Thomas HY, Ford Versypt AN. Pathophysiology of mesangial expansion in diabetic nephropathy: mesangial structure, glomerular biomechanics, and biochemical signaling and regulation. J Biol Eng. 2022;16:19.

6. Navarro-González JF, Mora-Fernández C, Muros de Fuentes M, García-Pérez J. Inflammatory molecules and pathways in the pathogenesis of diabetic nephropathy. Nat Rev Nephrol. 2011;7:327-40.

7. Tsalamandris S, Antonopoulos AS, Oikonomou E, Papamikroulis GA, Vogiatzi G, Papaioannou S, et al. The role of inflammation in diabetes: current concepts and future perspectives. Eur Cardiol. 2019;14:50-9.

8. Ayala TS, Tessaro FHG, Jannuzzi GP, Bella LM, Ferreira KS, Martins JO. High glucose environments interfere with bone marrow-derived macrophage inflammatory mediator release, the TLR4 pathway and glucose metabolism. Sci Rep. 2019;9:11447.

9. Galvão Tessaro FH, Ayala TS, Bella LM, Martins JO. Macrophages from a type 1 diabetes mouse model present dysregulated PI3K/AKT, ERK 1/2 and SAPK/JNK levels. Immunobiology. 2019;225:151879.

10. Rayego-Mateos S, Morgado-Pascual J, Opazo-Rios L, Guerrero-Hue M, García-Caballero C, Vázquez-Carballo C, et al. Pathogenic pathways and therapeutic approaches targeting inflammation in diabetic nephropathy. Int J Mol Sci. 2020;21:3798.

11. Alicic RZ, Rooney MT, Tuttle KR. Diabetic kidney disease: challenges, progress, and possibilities. Clin J Am Soc Nephrol. 2017;12:2032-45.

12. Johnson-Léger C, Imhof B. Forging the endothelium during inflammation: pushing at a half-open door? Cell Tissue Res. 2003;314:93-105.

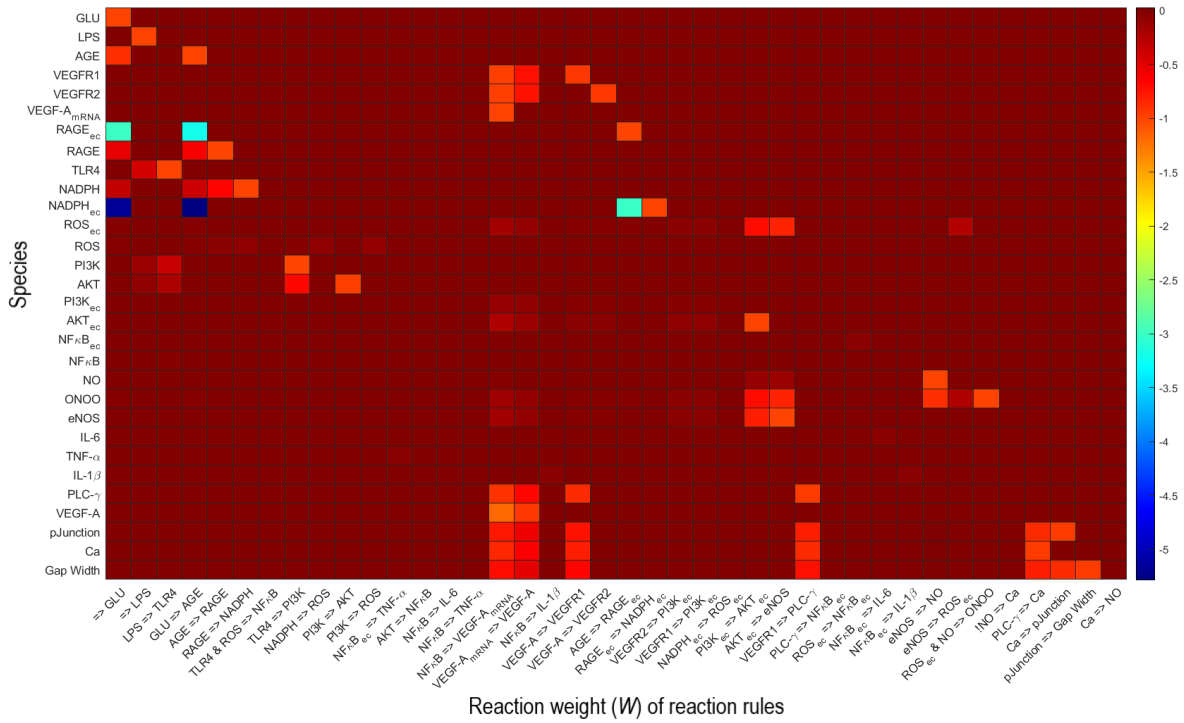

Figure A9: The local sensitivity index of change in output species (vertical axis) against the change in W parameters (horizontal axis). The horizontal axis is the reaction weight of the respective interaction rules. The color bar indicates the magnitude of the sensitivity index. The negative sign indicates a negative correlation between species output and the W parameter. GLU: glucose. LPS: lipopolysaccharide. TLR: toll-like receptor. AGE: advanced glycation end product. RAGE: receptor of advanced glycation end product. NADPH: nicotinamide adenine dinucleotide phosphate. NFκB: nuclear factor kappa B. IL: interleukin. TNF: tumor necrosis factor. PI3K: phosphoinositide 3-kinases. AKT: serine/threonine-specific protein kinases. ROS: reactive oxygen species. VEGF: vascular endothelial growth factor. VEGFR: vascular endothelial growth factor receptor. PLC: phospholipase C. NO: nitric oxide. ONOO: peroxynitrite. eNOS: endothelial nitric oxide synthase. Ca: calcium. pJunction: phosphorylated junction protein. Gap Width: change in endothelial cell gap width.

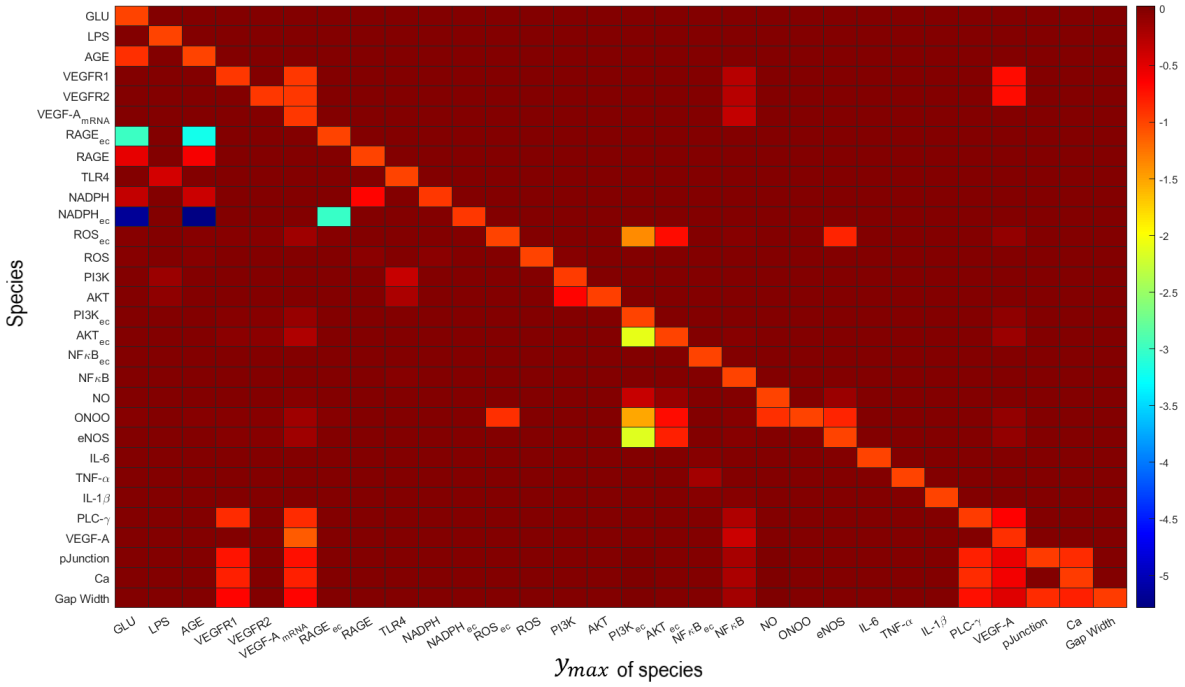

Figure A10: The local sensitivity index of change in output species (vertical axis) against the change in $y_{\max}$ parameters (horizontal axis). The color bar indicates the magnitude of the sensitivity index. The negative sign indicates a negative correlation between species output and $y_{\max}$ parameter. GLU: glucose. LPS: lipopolysaccharide. TLR: toll-like receptor. AGE: advanced glycation end product. RAGE: receptor of advanced glycation end product. NADPH: nicotinamide adenine dinucleotide phosphate. NFκB: nuclear factor kappa B. IL: interleukin. TNF: tumor necrosis factor. PI3K: phosphoinositide 3-kinases. AKT: serine/threonine-specific protein kinases. ROS: reactive oxygen species. VEGF: vascular endothelial growth factor. VEGFR: vascular endothelial growth factor receptor. PLC: phospholipase C. NO: nitric oxide. ONOO: peroxynitrite. eNOS: endothelial nitric oxide synthase. Ca: calcium. pJunction: phosphorylated junction protein. Gap Width: change in endothelial cell gap width.

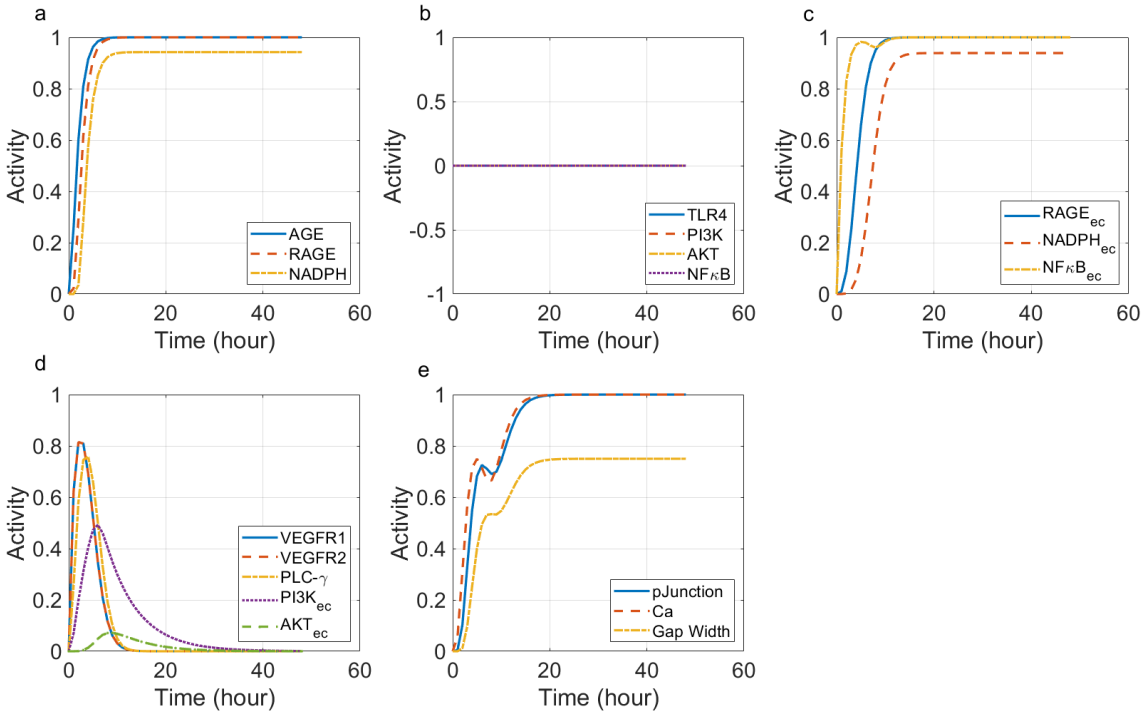

Figure A11: Species activity over 48 hours for all regulatory species in the network when stimulated with glucose (GLU). The subscript "ec" denotes intracellular expression in the glomerular endothelial cells. TLR: toll-like receptor. AGE: advanced glycation end product. RAGE: receptor of advanced glycation end product. NADPH: nicotinamide adenine dinucleotide phosphate. NFκB: nuclear factor kappa B. IL: interleukin. TNF: tumor necrosis factor. PI3K: phosphoinositide 3-kinases. AKT: serine/threonine-specific protein kinases. ROS: reactive oxygen species. VEGF: vascular endothelial growth factor. VEGFR: vascular endothelial growth factor receptor. PLC: phospholipase C. NO: nitric oxide. ONOO: peroxynitrite. eNOS: endothelial nitric oxide synthase. Ca: calcium. pJunction: phosphorylated junction protein. Gap Width: change in endothelial cell gap width.

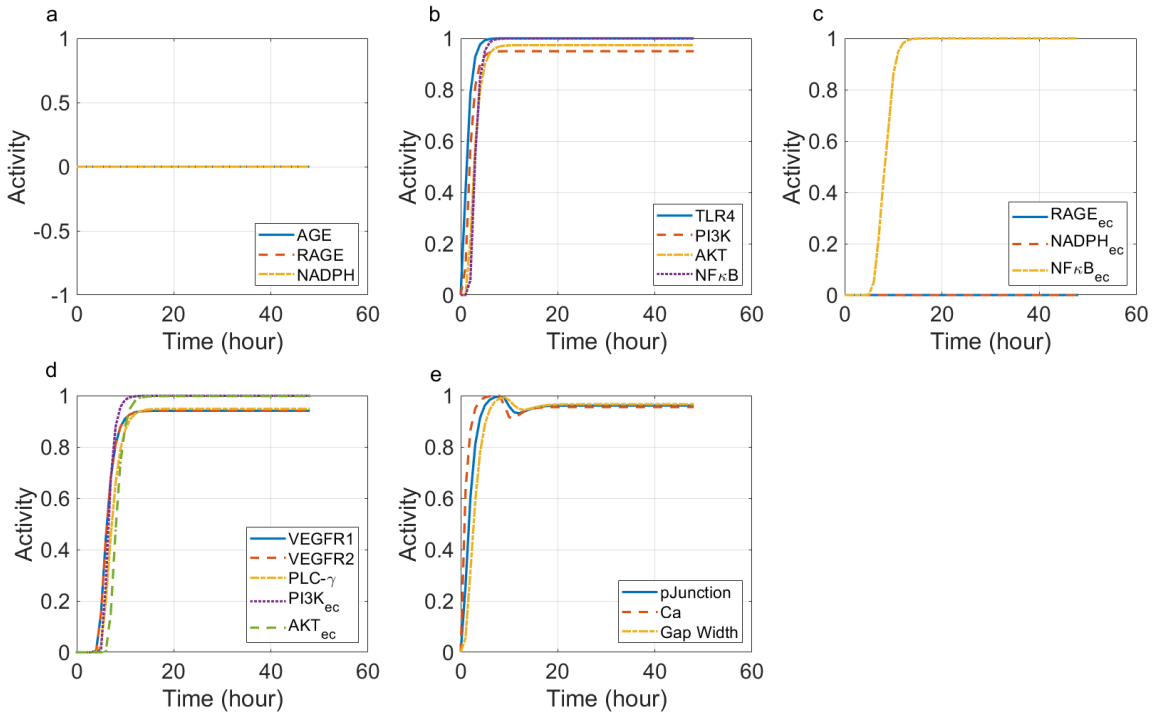

Figure A12: Species activity over 48 hours for all regulatory species in the network when stimulated with lipopolysaccharide (LPS). The subscript "ec" denotes intracellular expression within glomerular endothelial cells in the network. TLR: toll-like receptor. AGE: advanced glycation end product. RAGE: receptor of advanced glycation end product. NADPH: nicotinamide adenine dinucleotide phosphate. NFκB: nuclear factor kappa B. IL: interleukin. TNF: tumor necrosis factor. PI3K: phosphoinositide 3-kinases. AKT: serine/threonine-specific protein kinases. ROS: reactive oxygen species. VEGF: vascular endothelial growth factor. VEGFR: vascular endothelial growth factor receptor. PLC: phospholipase C. NO: nitric oxide. ONOO: peroxynitrite. eNOS: endothelial nitric oxide synthase. Ca: calcium. pJunction: phosphorylated junction protein. Gap Width: change in endothelial cell gap width.

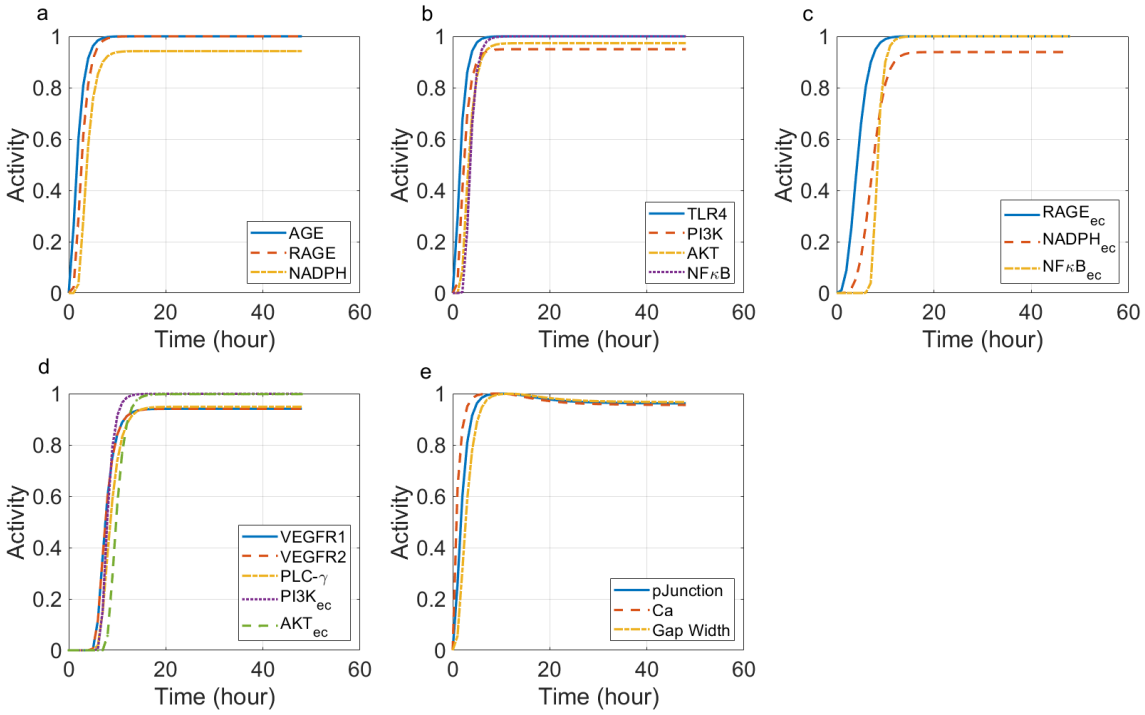

Figure A13: Species activity over 48 hours for all regulatory species in the network when stimulated with both glucose (GLU) and lipopolysaccharide (LPS). The subscript "ec" denotes intracellular expression within glomerular endothelial cells in the network. TLR: toll-like receptor. AGE: advanced glycation end product. RAGE: receptor of advanced glycation end product. NADPH: nicotinamide adenine dinucleotide phosphate. NFκB: nuclear factor kappa B. IL: interleukin. TNF: tumor necrosis factor. PI3K: phosphoinositide 3-kinases. AKT: serine/threonine-specific protein kinases. ROS: reactive oxygen species. VEGF: vascular endothelial growth factor. VEGFR: vascular endothelial growth factor receptor. PLC: phospholipase C. NO: nitric oxide. ONOO: peroxynitrite. eNOS: endothelial nitric oxide synthase. Ca: calcium. pJunction: phosphorylated junction protein. Gap Width: change in endothelial cell gap width.

13. Li Y, Yu W, He M, Yuan F. The effects of M1/M2 macrophages on the mRNA expression profile of diabetic glomerular endothelial cells. Nephron. 2021;145:1-11.

14. Takahashi T, Harris RC. Role of endothelial nitric oxide synthase in diabetic nephropathy: lessons from diabetic eNOS knockout mice. J Diabetes Res. 2014;2014:590541.

15. Wu Q, Finley S. Mathematical model predicts effective strategies to inhibit VEGF-eNOS signaling. J Clin Med. 2020;9:1255.

16. Zhao HJ, Wang S, Cheng H, Zhang MZ, Takahashi T, Fogo AB, et al. Endothelial nitric oxide synthase deficiency produces accelerated nephropathy in diabetic mice. J Am Soc Nephrol. 2006;17:2664-9.

17. Shu A, Du Q, Chen J, Gao Y, Zhu Y, Lv G, et al. Catalpol ameliorates endothelial dysfunction and inflammation in diabetic nephropathy via suppression of RAGE/RhoA/ROCK signaling pathway. Chem-Biol Interact. 2021;348:109625.

18. Bates DO. Vascular endothelial growth factors and vascular permeability. Cardiovasc Res. 2010;87:262-71.

19. Di Lorenzo A, Lin MI, Murata T, Landskroner-Eiger S, Schleicher M, Kothiya M, et al. eNOS-derived nitric oxide regulates endothelial barrier function through VE-cadherin and Rho GTPases. J Cell Sci. 2013;126:5541-52.

20. Satchell S, Tooke J. What is the mechanism of microalbuminuria in diabetes: a role for the glomerular endothelium? Diabetologia. 2008;51:714-25.

21. Satchell SC, Braet F. Glomerular endothelial cell fenestrations: an integral component of the glomerular filtration barrier. Am J Physiol Renal Physiol. 2009;296:F947-56.

22. Deen W, Lazzara M, Myers B. Structural determinants of glomerular permeability. Am J Physiol: Renal Physiol. 2001;281:F579-96.

23. Hostetter TH, Hauser EB, Daniels BS, Deen WM. Glomerular basement membrane: in vitro studies of water and protein permeability. Am J Physiol. 1992;262:F919-26.

24. Dechadilok P, Deen WM. Hindrance factors for diffusion and convection in pores. Ind Eng Chem Res. 2006;45:6953—6959.

25. Saez-Rodriguez J, Alexopoulos LG, Epperlein J, Samaga R, Lauffenburger DA, Klamt S, et al. Discrete logic modelling as a means to link protein signalling networks with functional analysis of mammalian signal transduction. Mol Syst Biol. 2009;5:331.

26. Ford Versypt AN, Harrell GK, McPeak AN. A pharmacokinetic/pharmacodynamic model of ACE inhibition of the renin-angiotensin system for normal and impaired renal function. Comput Chem Eng. 2017;104:311-22.

27. Pilvankar MR, Higgins MA, Ford Versypt AN. Mathematical model for glucose dependence of the local renin-angiotensin system in podocytes. Bull Math Biol. 2018;80(4):880-905.

28. Pilvankar MR, Yong HL, Ford Versypt AN. A glucose-dependent pharmacokinetic/pharmacodynamic model of ACE inhibition in kidney cells. Processes. 2019;7(3):131.

29. Ford Versypt AN. Multiscale modeling in disease. Curr Opin Syst Biol. 2021;27:100340.

30. Kraeutler MJ, Soltis AR, Saucerman JJ. Modeling cardiac β-adrenergic signaling with normalized-Hill differential equations: comparison with a biochemical model. BMC Syst Biol. 2010;4:157.

31. Weinstein N, Mendoza L, Gitler I, Klapp J. A network model to explore the effect of the micro-environment on endothelial cell behavior during angiogenesis. Front Physiol. 2017;8:960.

32. Saez-Rodriguez J, Simeoni L, Lindquist JA, Hemenway R, Bommhardt U, Arndt B, et al. A logical model provides insights into T cell receptor signaling. PLoS Comput Biol. 2007;3:e163.

33. Fu J, Akat K, Sun Z, Zhang W, Schlondorff D, Liu H, et al. Single-cell RNA profiling of glomerular cells shows dynamic changes in experimental diabetic kidney disease. J Am Soc Nephrol. 2019;30:533-45.

34. Selvaggio G, Cristellon S, Marchetti L. A Novel Hybrid Logic-ODE Modeling Approach to Overcome Knowledge Gaps. Front Mol Biosci. 2021;8.

35. Wittmann D, Krumsiek J, Saez-Rodriguez J, Lauffenburger D, Klamt S, Theis F. Transforming Boolean models to continuous models: Methodology and application to T-cell receptor signaling. BMC Syst Biol. 2009;3:98.

36. Krumsiek J, Pölsterl S, Wittmann D, Theis F. Odefy – From discrete to continuous models. BMC Bioinf. 2010;11:233.

37. Henriques D, Rocha M, Saez-Rodriguez J, Banga J. Reverse engineering of logic-based differential equation models using a mixed-integer dynamic optimisation approach. Bioinformatics. 2015;31.

38. Terfve C, Cokelaer T, Henriques D, MacNamara A, Goncalves E, Morris MK, et al. CellNOptR: A flexible toolkit to train protein signaling networks to data using multiple logic formalisms. BMC Syst Biol. 2012;6:133.

39. Afanasév I. Signaling of reactive oxygen and nitrogen species in diabetes mellitus. Oxid Med Cell Longevity. 2010;3:361-73.

40. Rendra E, Riabov V, Mossel DM, Sevastyanova T, Harmsen MC, Kzhyshkowska J. Reactive oxygen species (ROS) in macrophage activation and function in diabetes. Immunobiology. 2018;224:242-53.

41. Durán W, Breslin J, Sanchez F. The NO cascade, eNOS location, and microvascular permeability. Cardiovasc Res. 2010;87:254-61.

42. Shibuya M. Vascular endothelial growth factor receptor-1 (VEGFR-1/Flt-1): a dual regulator for angiogenesis. Angiogenesis. 2006;9:225-30.

43. Shibuya M. Structure and dual function of vascular endothelial growth factor receptor-1 (Flt-1). Int J Biochem Cell Biol. 2001;33:409-20.

44. Dalal P, Muller W, Sullivan D. Endothelial cell calcium signaling during barrier function and inflammation. Am J Pathol. 2019;190:535-42.

45. Singh VP, Bali A, Singh N, Jaggi AS. Advanced glycation end products and diabetic complications. Korean J Physiol Pharmacol. 2014;18:1-14.

46. Kanehisa M, Goto S. KEGG: kyoto encyclopedia of genes and genomes. Nucleic Acids Res. 2000;28:27-30.

47. Pico AR, Kelder T, van Iersel M P, Hanspers K, Conklin BR, C E. WikiPathways: pathway editing for the people. PLoS Biol. 2008;6:1-4.

48. Brooks D, Barr LC, Wiscombe S, McAuley DF, Simpson AJ, Rostron AJ. Human lipopolysaccharide models provide mechanistic and therapeutic insights into systemic and pulmonary inflammation. Eur Respir J. 2020;56:1901298.

49. Kanehisa M. Post-Genome Informatics. Kyoto University, Japan: Oxford University Press; 2000.

50. Paravicini TM, Touyz RM. NADPH oxidases, reactive oxygen species, and hypertension clinical implications and therapeutic possibilities. Diabetes Care. 2008;31:S170-80.

51. Koundouros N, Poulogiannis G. Phosphoinositide 3-kinase/Akt signaling and redox metabolism in cancer. Front Oncol. 2018;8:160.

52. Carranza K, Veron D, Cercado A, Bautista N, Pozo W, Tufro A, et al. Cellular and molecular aspects of diabetic nephropathy; the role of VEGF-A. Nefrologia. 2015;35:131-8.

53. Nakagawa T, Sato W, Kosugi T, Johnson RJ. Uncoupling of VEGF with endothelial NO as a potential mechanism for abnormal angiogenesis in the diabetic nephropathy. J Diabetes Res. 2013;2013:184539.

54. Warren CM, Ziyad S, Briot A, Der A, Iruela-Arispe ML. A ligand-independent VEGFR2 signaling pathway limits angiogenic responses in diabetes. Sci Signaling. 2014;7:ra1.

55. Yang KS, Lim JH, Kim TW, Kim MY, Kim Y, Chung S, et al. Vascular endothelial growth factor-receptor 1 inhibition aggravates diabetic nephropathy through eNOS signaling pathway in db/db mice. PloS One. 2014;9:e94540.

56. Imoukhuede PI, Dokun AO, Annnex BH, Popel AS. Endothelial cell-by-cell profiling reveals the temporal dynamics of VEGFR1 and VEGFR2 membrane localization after murine hindlimb ischemia. Am J Physiol Heart Circ Physiol. 2013;304:H1085-96.

57. Weddell JC, Imoukhuede PI. VEGFR1 promotes cell migration and proliferation through PLCγ and PI3K pathways. NPJ Syst Biol Appl. 2018;4:1.

58. Feliers D, Chen X, Akis N, Choudhury GG, Madaio M, Kasinath BS. VEGF regulation of endothelial nitric oxide synthase in glomerular endothelial cells. Kidney Int. 2005;68:1648-59.

59. Pinter E, Haigh J, Nagy A, Madri JA. Hyperglycemia-induced vasculopathy in the murine conceptus is mediated via reductions of VEGF-A expression and VEGF receptor activation. Am J Pathol. 2001;158:1199-206.

60. Ferraro M. Vascular endothelial growth factor: basic science and clinical progress. Endocr Rev. 2004;25:581-611.

61. Stan R, Tse D, Deharvengt S, Smits N, Xu Y, Luciano M, et al. The diaphragms of fenestrated endothelia: gatekeepers of vascular permeability and blood composition. Dev Cell. 2012;23:1203-18.

62. Nakagawa T, Sato W, Sautin YY, Glushakova O, Croker B, Atkinson MA, et al. Uncoupling of vascular endothelial growth factor with nitric oxide as a mechanism for diabetic vasculopathy. J Am Soc Nephrol. 2006;17:736-45.

63. de Souza LF, Barreto F, da Silva EG, Andrades ME, Guimarães ELM, Behr GA, et al. Regulation of LPS stimulated ROS production in peritoneal macrophages from alloxan-induced diabetic rats: involvement of high glucose and PPARγ. Life sciences. 2007;81:153-9.

64. Goers L, Freemont P, Polizzi K. Co-culture systems and technologies: taking synthetic biology to the next level. J R Soc Interface. 2014;11:96.

65. Kasai N, Sugimoto K, Horiba N, Suda T. Effect of D-glucose on nitric oxide release from glomerular endothelial cells. Diabetes/Metabolism Res Rev. 2001;17:217-22.

66. He S, Hu Q, Xu X, Niu Y, Chen Y, Lu Y, et al. Advanced glycation end products enhance M1 macrophage polarization by activating the MAPK pathway. Biochem Biophys Res Commun. 2020;525:334-40.

67. Yang Z, Mo X, Gong Q, Pan Q, Yang X, Cai W, et al. Critical effect of VEGF in the process of endothelial cell apoptosis induced by high glucose. Apoptosis. 2008;13:1331-43.

68. Seo JA, Sayyed ND, Lee YJ, Jeon HY, Kim EB, Hong SH, et al. Midazolam ameliorates hyperglycemia-induced glomerular endothelial dysfunction by inhibiting transglutaminase 2 in diabetes. Int J Mol Sci. 2022;23:753.

69. Ramanathan M, Giladi A, S LJ. Regulation of vascular endothelial growth factor gene expression in murine macrophages by nitric oxide and hypoxia. Exp Biol Med. 2003;228:697-705.

70. Du L, Dong F, Guo L, Yinglong H, Yi F, Liu J, et al. Interleukin-1β increases permeability and upregulates the expression of vascular endothelial-cadherin in human renal glomerular endothelial cells. Mol Med Rep. 2015;11:3708-14.

71. Rohatgi A. WebPlotdigitizer: Version 4.4; 2020. https://automeris.io/WebPlotDigitizer.

72. Abramoff MD, Magalhaes PJ, Ram SJ. Image processing with ImageJ. Biophotonics Int. 2004;11:36-42.

73. Makaryan S, Finley S. Enhancing network activation in natural killer cells: predictions from in silico modeling. Integr Biol. 2020;12:109-21.

74. Saucerman J. Netflux; 2015. https://github.com/saucermanlab/Netflux.

75. Cao S, Aboelkassem Y, Wang A, Valdez-Jasso D, Saucerman JJ, Omens JH, et al. Quantification of Model and Data Uncertainty in a Network Analysis of Cardiac Myocyte Mechanosignalling. 2020.

76. Prinz H. Hill coefficients, dose-response curves and allosteric mechanisms. J Chem Biol. 2009;3:37-44.

77. Villaverde AF, Tsiantis N, Banga JR. Full Observability and Estimation of Unknown Inputs, States and Parameters of Nonlinear Biological Models". 2019.

78. Hass H, Kreutz C, Timmer J, Kaschek D. Fast integration-based prediction bands for ordinary differential equation models. Bioinformatics (Oxford, England). 2015;32.

79. Díaz-Seoane S, Rey Barreiro X, Villaverde AF. STRIKE-GOLDD 4.0: user-friendly, efficient analysis of structural identifiability and observability. Bioinformatics. 2022;39(1):btac748.

80. Ciupe S, Tuncer N. Identifiability of parameters in mathematical models of SARS-CoV-2 infections in humans. Scientific Reports. 2022;12.

81. Villaverde AF. STRIKE-GOLDD v4.0 user manual; 2022. http://afvillaverde.webs.uvigo.gal/.

82. Marelli S, Sudret B. UQLab: A Framework for Uncertainty Quantification in MATLAB. In The 2nd International Conference on Vulnerability and Risk Analysis and Management (ICVRAM 2014):2014.

83. Marelli S, Lamas C, Konakli K, Mylonas C, Wiederkehr P, Sudret B. UQLab user manual – Sensitivity analysis; 2022. Report UQLab-V2.0-106.

84. Linden NJ, Kramer B, Rangamani P. Bayesian parameter estimation for dynamical models in systems biology. PLOS Computational Biology. 2022;18(10):1-48.

85. Marino S, Hogue I, Ray C, Kirschner D. A methodology for performing global uncertainty and sensitivity analysis in systems biology. J Theor Biol. 2008;254:178-96.

86. Wang RS, Saadatpour A, Albert R. Boolean modeling in systems biology: an overview of methodology and applications. Phys Biol. 2012;9:055001.

87. RStudio Team. RStudio: Integrated Development Environment in R; 2020. http://www.rstudio.com/.

88. The MathWorks Inc . MATLAB version 9.11.0.1809720 (R2021b) Update 1; 2021. https://www.mathworks.com/.

89. Itaya H, Imaizumi T, Yoshida H, Koyama M, Suzuki S, Satoh K. Expression of vascular endothelial growth factor in human monocyte/macrophages stimulated with lipopolysaccharide. Thromb Haemostasis. 2001;85:171-6.

90. Rex J, Albrecht U, Ehlting C, Thomas M, Zanger U, Sawodny O, et al. Model-based characterization of inflammatory gene expression patterns of activated macrophages. PLoS Comput Biol. 2016;12:e1005018.

91. Patidar K, Ford Versypt AN. KidneyImmuneLBM; 2023. https://github.com/ashleefv/KidneyImmuneLBM. DOI: 10.5281/zenodo.7958230.